EFFECTS OF CONSTRAINED AGING ON THE SHAPE MEMORY RESPONSE OF NICKEL RICH NITI SHAPE MEMORY ALLOYS

A Thesis

by

FATMATA HAJA BARRIE

Submitted to the Office of Graduate Studies of
Texas A&M University
in partial fulfillment of the requirements for the degree of

MASTER OF SCIENCE

December 2009

Major Subject: Mechanical Engineering

EFFECTS OF CONSTRAINED AGING ON THE SHAPE MEMORY RESPONSE OF NICKEL RICH NITI SHAPE MEMORY ALLOYS

A Thesis

by

FATMATA HAJA BARRIE

Submitted to the Office of Graduate Studies of
Texas A&M University
in partial fulfillment of the requirements for the degree of

MASTER OF SCIENCE

Approved by:

Chair of Committee,	Ibrahim Karaman
Committee Members,	Richard Griffin
	Aydin Karsilayan
Head of Department,	Dennis O'Neal

December 2009

Major Subject: Mechanical Engineering

ABSTRACT

Effects of Constrained Aging on the Shape Memory Response

of Nickel Rich NiTi Shape Memory Alloys. (December 2009)

Fatmata Haja Barrie, B.S., Carnegie Mellon University

Chair of Advisory Committee: Dr. Ibrahim Karaman

$Ni_{50.6}Ti_{49.4}$ single and $Ni_{52}Ti_{48}$ polycrystalline shape memory alloy samples were subjected to aging under a uniaxial stress, to form a single Ni_4Ti_3 precipitate variant and to investigate the effects of single versus multi-variant coherent precipitates on the shape memory characteristics including two-way shape memory effect (TWSME). Shape memory and superelasticity properties along with the effects of stress and temperature on the transformation temperatures, strain, hysteresis, dimensional stability, and R-phase formation were investigated. This was accomplished through the use of isobaric thermal cycling and superelasticity experiments and various microscopy techniques that included transmission electron microscopy (TEM), scanning electron microscopy, and optical microcopy.

The results showed that it is feasible to use constrained aging to bias R-phase martensite variants upon cooling from austenite without any external stress, however, accomplishing this with B19'martensite was much harder as complete TWSME was only found in the $Ni_{50.6}Ti_{49.4}$ single crystalline sample oriented along the $[\bar{1}12]$ direction. The onset of irrecoverable strain corresponded to the R-phase temperature hysteresis

increase in the single crystalline samples regardless of the aging conditions. Through TEM analysis it was discovered that [112] and [114] twins were found in austenite due to plastic deformation of martensite during the superelasticity experiments. Since [112] twins are theoretically impossible to form in austenite, and since martensite was plastically deformed, [112] austenite twins were attributed to the transformation of compound twins in martensite, in particular [113] martensite twins formed during the plastic deformation of martensite, into austenite twins.

In the $Ni_{52}Ti_{48}$ polycrystalline samples, a compressive R-phase variant was biased through constrained aging under 100 and 200 MPa uniaxial tensile stresses at 400°C and 450°C. Aging, in all conditions, produced a high density of Ni_4Ti_3 precipitates that was most likely responsible for the small transformation strain observed, less that 2%, upon transformation to martensite.

In the future, samples with compositions between 50.8 and 51.5 Ni atomic percent, in addition to altered solution and aging heat treatments as compared to those used in this study should be investigated as it is believed that samples with these compositions will yield better and consistent TWSME responses through constrained aging.

DEDICATION

This thesis is dedicated to my mother and father

ACKNOWLEDGEMENTS

I would like to give a special thanks to my mother, father, sister, and brother for their encouragement. I would also like to thank my committee chair, Dr. Karaman, and my committee members, Dr. Griffin and Dr. Karsilayan, for their guidance throughout the course of this research.

Thanks also go to Professor Chumlyakov and Dr. Kireeva for the informative discussions, samples for use in part of this study and for help in producing the TEM images shown in parts of this thesis.

NOMENCLATURE

A_s	Austenite Transformation Start Temperature
A_f	Austenite Transformation Finish Temperature
BCC	Body Centered Cubic
M_s	Martensite Transformation Start Temperature
M_f	Martensite Transformation Finish Temperature
NiTi	Nickel Titanium
OM	Optical Microscopy
R_s	R-phase Transformation Start Temperature
R_f	R-phase Transformation Finish Temperature
SMA	Shape Memory Alloy
SEM	Scanning Electron Microscopy
TEM	Transmission Electronic Microscopy
TWSME	Two-way Shape Memory Effect

TABLE OF CONTENTS

Page

ABSTRACT iii

DEDICATION v

ACKNOWLEDGEMENTS vi

NOMENCLATURE vii

TABLE OF CONTENTS viii

LIST OF FIGURES x

LIST OF TABLES xiii

CHAPTER

I INTRODUCTION 1

Background 1
Motivation 7
Objectives 8

II EXPERIMENTAL PROCEDURES 9

Single Crystalline Sample Preparation 9
Polycrystalline Sample Preparation 11
Isobaric Thermal Cycling Experiments 12
Superelasticity Experiments 14
Optical Microscopy and Transmission Electron Microscopy 15

III EFFECT OF AGING ON SINGLE CRYSTALLINE $Ni_{50.6}Ti_{49.4}$SMAs 16

Isobaric Thermal Cycling Experimental Results and Analysis 16
Superelasticity Experimental Results and Analysis 35

CHAPTER Page

IV EFFECT OF AGING ON POLYCRYSTALLINE $Ni_{52}Ti_{48}$ SMAs..... 44

Isobaric Thermal Cycling Experimental Results and Analysis..... 44
Microstructural Investigation 64

V SUMMARY AND CONCLUSIONS..... 70

Single Crystalline $Ni_{50.6}Ti_{49.4}$ 70
Polycrystalline $Ni_{52}Ti_{48}$ 71

VI FUTURE WORK..... 73

REFERENCES..... 74

VITA 76

LIST OF FIGURES

FIGURE		Page
1	The SMA shape recovery mechanism is a result of various solid-to-solid phase transformations	2
2	This schematic shows the possible effects of aging NiTi SMAs under a) no, b) compressive, and c) tensile bias stresses	5
3	Dog-bone shaped tensile samples were cut from the hot-rolled plate	9
4	This schematic shows how the start and finish transformation temperatures were determined as well as the temperature hysteresis, and total transformation strain	14
5	Isobaric thermal cycling experimental results for the single crystalline $Ni_{50.6}Ti_{49.4}$ samples aged under a) no constraint, b) tension, and c) compression	16
6	Resulting R-phase and martensite temperature hysteresis response from the isobaric thermal cycling experiments for the $Ni_{50.6}Ti_{49.4}$ single crystalline samples	20
7	Strain-temperature curve response from the isobaric load bias experiments for $Ni_{50.6}Ti_{49.4}$ single crystal samples under 0 MPa	21
8	Stress vs. temperature phase diagram of $Ni_{50.6}Ti_{49.4}$ single crystal along the [112] orientation	25
9	Strain-temperature response for the $Ni_{50.6}Ti_{49.4}$ single crystalline samples at a) 100 MPa and b) 300 MPa	31
10	Resulting a) R-phase transformation, total transformation and b) irrecoverable strains from the $Ni_{50.6}Ti_{49.4}$ single crystal samples from the isobaric thermal cycling experiments	33
11	Sample A, aged under no constraint, single crystal $Ni_{50.6}Ti_{49.4}$ stretched at incremental strains up to 17% at 50°C	36
12	OM images of deformation twins produced during the superelasticity experiments	39

FIGURE Page

13 A compilation of TEM images of the deformation twins produced during the superelasticity experiments 40

14 TEM images from a) sample A and b) sample B showing the coherency stresses produced by the presence of Ni_4Ti_3 precipitates..... 41

15 Bright field TEM image and corresponding diffraction pattern of sample B showing aligned R-phase variants 43

16 Isobaric thermal cycling experimental results for the polycrystalline $Ni_{52}Ti_{48}$ samples that were aged under no constraint.. 45

17 Isobaric thermal cycling experimental results for the polycrystalline $Ni_{52}Ti_{48}$ samples that were solution treated at 850°C for 1 hr then furnace cooled for 12 hrs 47

18 Isobaric thermal cycling experimental results for the polycrystalline $Ni_{52}Ti_{48}$ sample that was hot-rolled then aged at 450°C for 5hrs under a 200 MPa tensile stress 49

19 Strain-temperature curve results from the isobaric load bias experiments for $Ni_{52}Ti_{48}$ polycrystalline samples under 0 MPa 53

20 Strain-temperature curve results from the isobaric load bias experiments for $Ni_{52}Ti_{48}$ polycrystalline samples under 0 MPa with samples 6-9 superimposed for easier comparison 54

21 Stress vs. temperature phase diagram of $Ni_{52}Ti_{48}$ polycrystalline samples 1, 2, and 5.. 55

22 Stress vs. temperature phase diagram of $Ni_{52}Ti_{48}$ polycrystalline samples 3 and 4 58

23 Stress vs. temperature phase diagram of $Ni_{52}Ti_{48}$ polycrystalline sample 6..... 60

24 R-phase transformation strains for samples 2, 5, and 6 of the $Ni_{52}Ti_{48}$ polycrystalline samples 62

25 Temperature hysteresis values for samples 1-6 of the $Ni_{52}Ti_{48}$ polycrystalline samples 63

FIGURE Page

26 Total transformation strains for samples 1-6 of the $Ni_{52}Ti_{48}$ polycrystalline samples 65

27 Irrecoverable strains experienced by samples 1-6 of the $Ni_{52}Ti_{48}$ polycrystalline samples 65

28 SEM images taken of the a) hot-rolled (as-received) sample and b) 900°C solution heat treated water quenched sample..... 66

29 SEM image of $Ni_{52}Ti_{48}$ polycrystalline samples a) 1 and b) 2..... 68

LIST OF TABLES

TABLE		Page
1	Different constrained aging treatments applied to the single crystal samples with the nominal composition of $Ni_{50.6}Ti_{49.4}$ used in this study	10
2	Different aging treatments applied to the polycrystalline samples with the nominal composition of $Ni_{52}Ti_{48}$	12
3	During stage IV of the 50°C superelasticity test, sample A began to experience significant irrecoverable strain	37

CHAPTER I

INTRODUCTION

Background

Shape memory alloys (SMAs) are a class of metals first reported in 1932 by Arne Ölande who witnessed shape memory behavior in Au-Cd [1]. SMAs differ from conventional metals, such as steel and aluminum, by their ability to return to a remembered shape after deformation. However, it was not until 1968, when NiTi was discovered by William Buehler of the Naval Ordinance Laboratory, that SMAs really became popular. Today, NiTi is the most common commercially used and investigated SMA. NiTi is widely studied because of its attractive physical and mechanical properties that include corrosion and fatigue resistance, biocompatibility, and ductility in addition to shape memory and superelasticity. Applications include eyeglasses frames, cellular phone antennas, and a number of actuator uses that include shaping airplane wings.

The shape memory mechanism is caused by reversible solid-to-solid structural transformations that are temperature and stress dependent. Multiple phases, each with their unique corresponding crystal structure, exist. The transforming phases are called austenite and martensite. Austenite is the high symmetry high temperature phase and has a B2 body centered cubic (BCC) crystal structure in NiTi. Characteristically,

---

This thesis follows the style of Scripta Materialia.

martensite is a low symmetry low temperature phase. Martensite can be stress induced, per loading of the austenite phase. Several types of martensite exist. Those found in NiTi include B19' martensite and R-phase martensite, with monoclinic and rhombohedral crystal structures, respectively. Figure 1 shows each of the unit cells. The temperatures at which each crystal structure begins and ends forming is known as the start and finish transformation temperatures, respectively. In the case of austenite, for example, this would be the austenite start, A_s, and austenite finish, A_f, transformation temperatures. The actual temperatures vary based on the specific crystal structure and thermo-mechanical deformation history. [2]

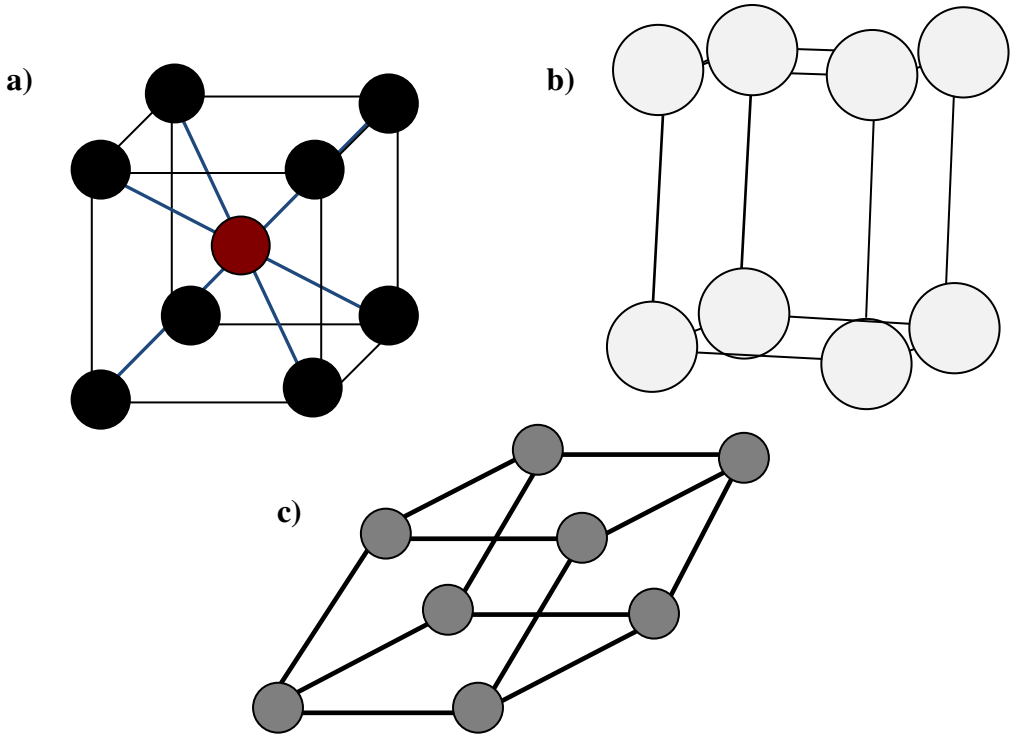

Figure 1. The SMA shape recovery mechanism is a result of various solid-to-solid phase transformations. This figure shows NiTi related unit cells for the a) B2 BCC, b) monoclinic, and c) rhombohedral crystal structures for the B2 austenite, B19' martensite, and R-phase, respectively.

Intrinsic SMA properties include superelasticity and shape memory effect. An external deformation applied in the austenite phase results in superelasticity. Superelasticity occurs when a perceived inelastic strain is fully recovered upon removal of an applied external load. This type of martensite is known as stress induced martensite.

Shape memory effect results in full strain recovery after an apparent inelastic deformation, caused by an applied external load, while the SMA is in a martensitic phase. Strain recovery occurs once the SMA is heated above its austenite transformation temperature. When a SMA is cooled without any external deformation, a self accommodated martensite forms. This self accommodated martensite twins in order to take the shape of the material in the austenite phase thereby producing no detectable macroscopic shape change. When a significant stress is applied to the SMA this results in the detwinning. Detwinning is the growth of one martensite variant, or configuration, at the expense of others. The detwinning process is fully reversible and is capable of producing transformation strains up to 10% depending on the magnitude of external stress applied, SMA heat treatment history, and the crystallographic texture of the sample tested, upon reverse transformation to austenite. The amount of detwinning increases with applied stress and it is seen during both superelasticity and shape memory effect experiments. [3,4]

A material that experiences two way shape memory effect (TWSME) is capable of undergoing a detectable transformation strain under zero applied stress. This occurs

when internal stresses, often caused by the presence of precipitates or oriented dislocations, bias one martensite variant enabling the material to remember two different shapes, one at low temperatures in the martensite phase in addition to the customary high temperature shape in the austenite phase. [4]

A number of thermo-mechanical treatments can generate necessary internal stresses to induce TWSME. Many involve a combination of numerous temperature, deformation, and/or stress cycling to induce specific martensite variants [4]. Fortunately, constrained aging, or aging under an applied external stress, serves as an attractive preparation technique by reducing the need for time consuming and costly thermo-mechanical training in applications.

Aging in NiTi can possibly produce Ti_3Ni_4, Ti_2Ni_3, and $TiNi_3$ precipitates, however prior research has shown that in its coherent form, Ti_3Ni_4 is responsible for affecting SMA transformation and TWSME behavior [2,5]. The precipitates are non-transformable and in their coherent state, the difference between the crystal structures of the precipitates and the matrix produce the internal stress fields around them.

The nickel composition of NiTi heavily influences the ability to successfully undergo constrained aging to produce TWSME. NiTi SMAs can be classified into two categories, near equi-atomic compositions with compositions near 50 atomic percent nickel, and nickel rich compositions, compositions having 50.6 atomic percent or more

of nickel. Nickel composition largely affects the transformation behavior of SMAs by changing the temperatures at which the solid-to-solid phase transformations occur. Aged, near equi-atomic NiTi SMAs have a lower Ni_4Ti_3 precipitate density than their Ni-rich counterparts. [6,7,8] The low precipitate density results in an insufficient amount of internal stress that is incapable of producing TWSME. When a sample is aged in the free condition, four precipitate variants are produced, however, prior research has shown that a single variant is created when a compressive or tensile stress between 50 MPa and 300 MPa is applied to the sample during aging. [6,7,9-11] Figure 2 shows the perceived effects of the tensile and compressive bias stresses applied during aging of NiTi SMAs.

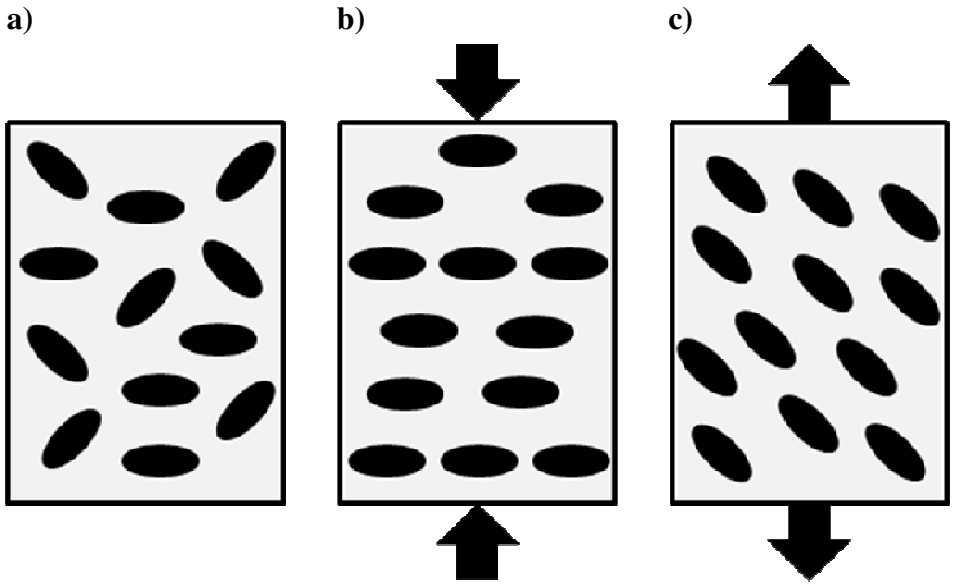

Figure 2. This schematic shows the possible effects of aging NiTi SMAs under a) no, b) compressive, and c) tensile bias stresses**.**

In addition to influencing transformation temperatures, aging, along with grain boundary refinement, texture strengthening, strain hardening, and solid solution strengthening, serve as strengthening mechanisms, effectively improving the material's resistance to plastic deformation. In SMAs, plastic deformation accompanying martensitic transformation is manifested as irrecoverable strain that develops during forward and/or reverse transformations. Consequently, the dimensional stability, or the alloy's ability to retain its shape during thermo-mechanical cycling, is vital to avoiding performance degradation. Aging provides the most effective strengthening mechanism in Ni-rich NiTi SMAs, pending the Ni_4Ti_3 precipitates are the precipitate form.

In NiTi, B19' martensite is capable of producing transformation strains of up to 10% depending on the sample condition and texture, and the thermo-mechanical deformation history. R-phase, on the other hand, can only result in transformation strains up to approximately 1% [12]. Additionally, the R-phase hysteresis is significantly smaller than that of the B19' hysteresis. Thus, the R-phase transformation is suited for small amplitude actuator and damping applications, especially those requiring a large number of cycles and higher efficiency. R-phase and B19' martensite can coexist at lower stress levels, however, after a critical stress has been applied, the R-phase subsides leaving only the B19' phase. Not all NiTi SMAs are capable of undergoing R-phase transformations. The R-phase is seen when the B19' martensite start temperature is suppressed. The R-phase can form under the following conditions: 1) cold working followed by annealing at low temperatures, 2) addition of a third element such as iron,

and 3) aging samples between 300 and 500°C. [13, 14] Aging appears to be the most promising due to its other benefit as a strengthening mechanism.

Motivation

As with any material, resistance to plastic deformation is imperative for use in practical applications. Since coherent Ti_3Ni_4 precipitates can be produced during select aging processes, the dimensional stability is increased thus, increasing the stress level at which permanent plastic deformation occurs. The formation of the Ti_3Ni_4 precipitate during aging also allows for customizable transformation temperatures due to the depletion of Ni in the matrix. [15] Since conventional methods used to produce TWSME in NiTi are costly and time consuming, in the present study, experimental work is conducted to better understand the effects of different constraint conditions during aging on the TWSME, shape memory properties and R-phase formation of Ni-rich NiTi SMA samples.

Objectives

The following are the present work's objectives:

1) To determine effective heat treatments that produce TWSME in Ni-rich NiTi SMAs

2) To investigate the effects of aging on the shape memory effect and superelasticity properties on Ni-rich NiTi SMAs

3) To investigate the effects of different heat treatments on the formation of R-phase martensite

4) To investigate the effect of various heat treatments on the dimensional stability of NiTi SMAs.

CHAPTER II

EXPERIMENTAL PROCEDURES

Single Crystalline Sample Preparation

Single crystalline samples of Ti-50.6 at%Ni (Ti-56 wt%Ni) nominal composition oriented along the [112] direction were prepared using the Bridgman method in an inert gas atmosphere [9]. The samples were then cut into tensile specimens similar to the one shown in Figure 3. The thicknesses of the samples A, B, and C were 1.22 mm, 0.8 mm, and 2.63 mm, respectively.

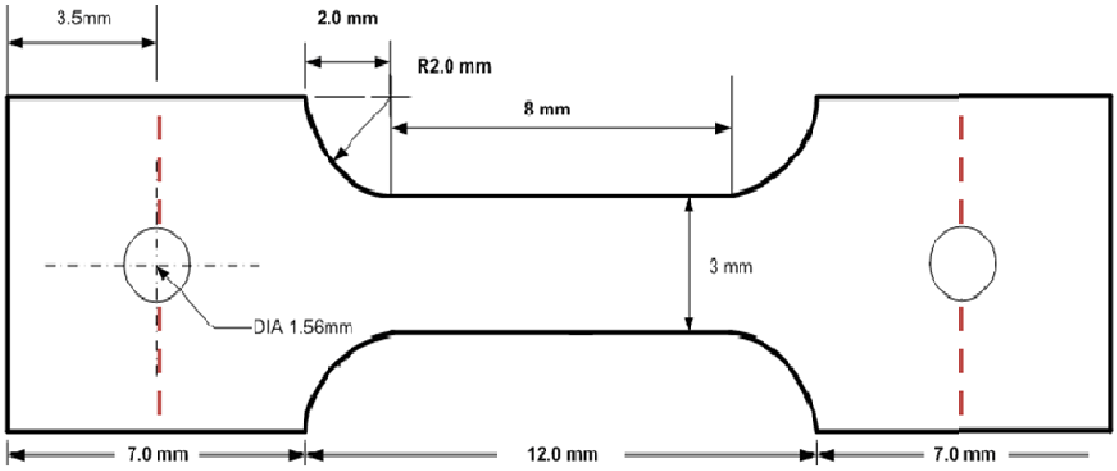

Figure 3. Dog-bone shaped tensile samples were cut from the hot-rolled plate.

The Bridgman method often leaves the sample compositionally nonuniform; therefore, the samples were homogenized at 950°C for 1 hour then water quenched and subsequently aged at 400°C for 1.5 hours under no stress, tension, or compression at 150 MPa producing Ti_3Ni_4 precipitates. Table 1 shows the sample heat treatment histories.

Table 1. Different constrained aging treatments applied to the single crystal samples with the nominal composition of $Ni_{50.6}Ti_{49.4}$ used in this study.

	Homogenization		Aging			
Sample	Temperature (° C)	Time (hr)	Temperature (° C)	Time (hr)	Stress (MPa)	Stress Type
A	950	1	400	1.5	0	--
B	950	1	400	1.5	150	tensile
C	950	1	400	1.5	150	compressive

Two different conditions of sample C were tested. The first was prepared in concurrence with samples A and B will be referred to as sample C1. The second sample was prepared independently of samples A, B, and C1. This sample is oriented along the [T12] direction, and will be referred to as sample C2.

Single crystals were used due to eliminate grain boundary effects thus allowing for an uncomplicated investigation of precipitate effects. The $Ni_{50.6}Ti_{49.4}$ composition was selected because these samples exhibit more ductility than higher Ni concentrated samples. The aging stress was selected because compressive and tensile stressed between 50 MPa and 300 MPa were shown to produce single precipitate variants in NiTi [10,15]. For this reason, 150 MPa aging stresses were selected to produce TWSME. The [112] orientation was selected based on Li and Chen's theoretical findings that showed only certain oriented aging stresses resulted in single precipitant variants. The [112] direction was in this category. [16] The aging temperature and time were selected

because similar alloy compositions aged at the same temperature and time have been shown to produce peak-aged alloys with coherent precipitates. [16-18] Samples heated between 400°C and 500°C for durations between 1 and 1.5 hrs for $Ni_{50.8at}Ti$ produce peak aged materials. The peak aged samples possess coherent and/or semi-coherent precipitates which create internal stresses within the samples. [19] These internal stresses were expected to produce TWSME.

Polycrystalline Sample Preparation

$Ni_{52}Ti_{48}$ polycrystalline plates were initially received in hot-rolled condition. Samples were then EDM cut into standard 1 -1.5 mm thick dog-bone shaped tensile samples, shown in Figure 3, with the rolling direction along the tensile axis. Table 2 shows the solution heat treatment and aging conditions used for these polycrystalline tension samples.

Solution heat treatment refers to the process of dissolving precipitate phases created during the casting and/or hot-rolling process without melting the matrix. The solution heat treatment temperatures were selected based on the binary NiTi phase diagram. 850°C and 900°C lie in the single TiNi phase region for the $Ni_{52}Ti_{48}$ composition, or above the solvus temperature of 812 ± 22°C. [20] Solution heat treating the samples at these temperatures achieves the desired effects i.e. dissolves the precipitates. The aging temperature was selected based on unpublished results from NASA Glenn Research

Center that indicated aging at 450°C for at least 5 hours produced the highest hardness from the aging regimes tested indicative of the peak aged condition.

Table 2. Different aging treatments applied to the polycrystalline samples with the nominal composition of $Ni_{52}Ti_{48}$. All samples were initially hot-rolled. The two cooling rates were either water quenched, WQ, and furnace cooled for 12 hours, FC.

	Solution Heat Treatment			Aging			
Sample	Temperature (°C)	Time (hr)	Cooling Rate	Temperature (°C)	Time (hr)	Stress (MPa)	Stress Type
1	--	--	--	--	0	0	--
2	--	--	--	450	5	0	--
3	850	1	FC	--	0	0	--
4	850	1	FC	450	5	0	--
5	900	1	WQ	450	5	0	--
6	--	--	--	450	5	200	tensile
7	900	1	WQ	450	5	200	tensile
8	900	1	WQ	450	5	100	tensile
9	900	1	WQ	400	24	200	tensile

The 200 MPa tensile stress was selected because it falls within the 50 MPa to 300 MPa tensile or compressive stress range shown to produce a single precipitant variant. The polycrystalline samples were used because they are more practical and much less expensive than single crystalline samples.

Isobaric Thermal Cycling Experiments

The isobaric thermal cycling experiments were performed on a MTS servo-hydraulic load frame. Each sample was cycled once between approximately 100° C and -60°C at

constant uniaxial tensile stress levels at a heating/cooling rate of 10°C per minute. For a certain number of tests, the samples were cycled between 100 and 20°C to selectively observe the R-phase characteristics. The stress levels were increased incrementally as follows 0, 25, 50, 75, 100, 150, 200, 250, 300, 350, 400, 450, and 500 MPa, or until the sample showed significant irrecoverable strain, to have a good understanding of the transformation behaviors. The stress was increased at the 100°C maximum temperature of each cycle. The strain was measured using an extensometer with a 0.5 inch gage length. The sample temperature was measure using a type K thermocouple attached to the center of the gage section of the sample.

From resulting data, strain versus temperature plots were produced. Austenite, R-phase, and martensite start and finish temperatures were derived to produce stress versus temperature phase diagrams. The precise start and finish temperature of each transformation are unknown, however by using the Tangent method, an accepted method for determining the temperatures in SMA literature, transformation temperatures were found. The temperature hysteresis was determined by taking the temperature difference at the point of 50% transformation completion. The transformation strain was determined by taking the strain difference between a point prior to and following transformation during cooling. The irrecoverable strain was found by taking the difference between the finish and start strain values. Figure 4 shows how the start and finish temperatures, temperature hysteresis, total transformation strain, and irrecoverable strain values were found.

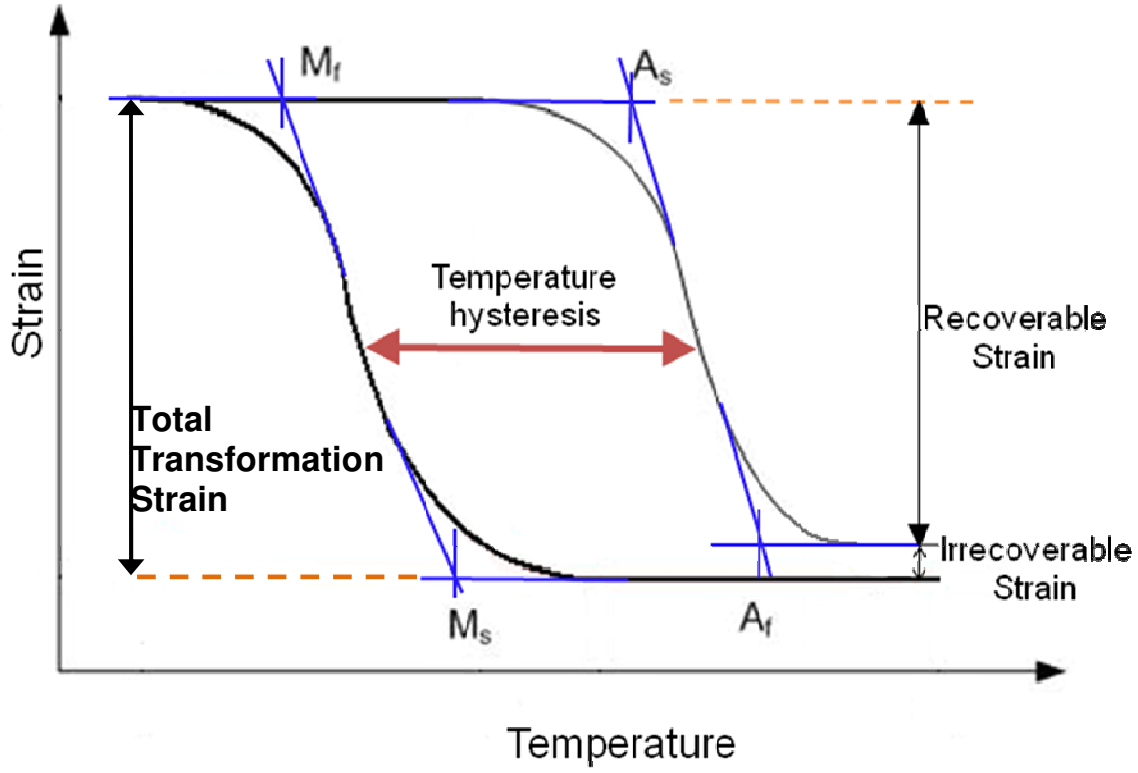

Figure 4. This schematic shows how the start and finish transformation temperatures were determined as well as the temperature hysteresis, and total transformation strain.

Superelasticity Experiments

The superelasticity experiments were also performed on the same MTS servo-hydraulic load frame with the strain being measured with a 0.5 inch gage length extensometer. The phase diagram derived from the isobaric thermal cycling experiments was used to determine the minimum temperature at which austenite existed. The sample was loaded in increments or either 1% or 2% of the original strain, at a 6 x 10^{-3} s^{-1} at various temperatures above the minimum austenite temperature until the plastic deformation

region of the sample was captured. This was repeated at various temperatures until sample failure. From the stress-strain results, the irrecoverable strain was found by taking the difference between the finish and start strain values. The results were then correlated to the optical microscopy and TEM images.

Optical Microscopy and Transmission Electron Microscopy

Following the isobaric thermal cycling and superelasticity experiments, a digital Keyence VH-Z100 optical microscope and JEOL JEM-2010 TEM operated at 200 kV accelerating voltage were used to examine the microstructural characteristics of the samples. To prepare the samples for optical microscopy, the sample surfaces were mechanically polished using SiC polishing paper and alumina powder mixtures down to a 0.5 μm final polish. The samples were then chemically etched in a 3 HNO_3 + 2 H_2O + 1 HF, in part, solution.

Thin films were prepared from the deformed and un-deformed regions of the etched samples for TEM preparation. The deformed region refers to the part of the sample that was externally stressed during the isobaric thermal experiments, or the gage section. The un-deformed region refers to the part of the sample unstressed by an external load during the isobaric tests. Figure 3, above, shows the deformed and un-deformed regions of the tensile sample. The thin films were electro-polished using a 20 vol.% H_2SO_4 and 80 vol.% methanol electro-polishing solution. TEM images were taken of different areas of the samples, at room temperature.

CHAPTER III

EFFECT OF AGING ON SINGLE CRYSTALLINE $Ni_{50.6}Ti_{49.4}$ SMAs

Isobaric Thermal Cycling Experimental Results and Analysis

Figure 5 shows the results of the isobaric thermal cycling experiments. The figure shows that temperature cycling caused each sample to undergo B2 to R-phase and followed by an R-phase to B19' martensite transformations during the forward transformation. During the reverse transformation, R-phase was only seen in samples A and C1, in samples B and C2 B19' martensite transformed directly to B2 austenite. It is likely that samples, under low stress levels, transforms to the R-phase but the transformations occur very close to one another, making them appear indistinguishable.

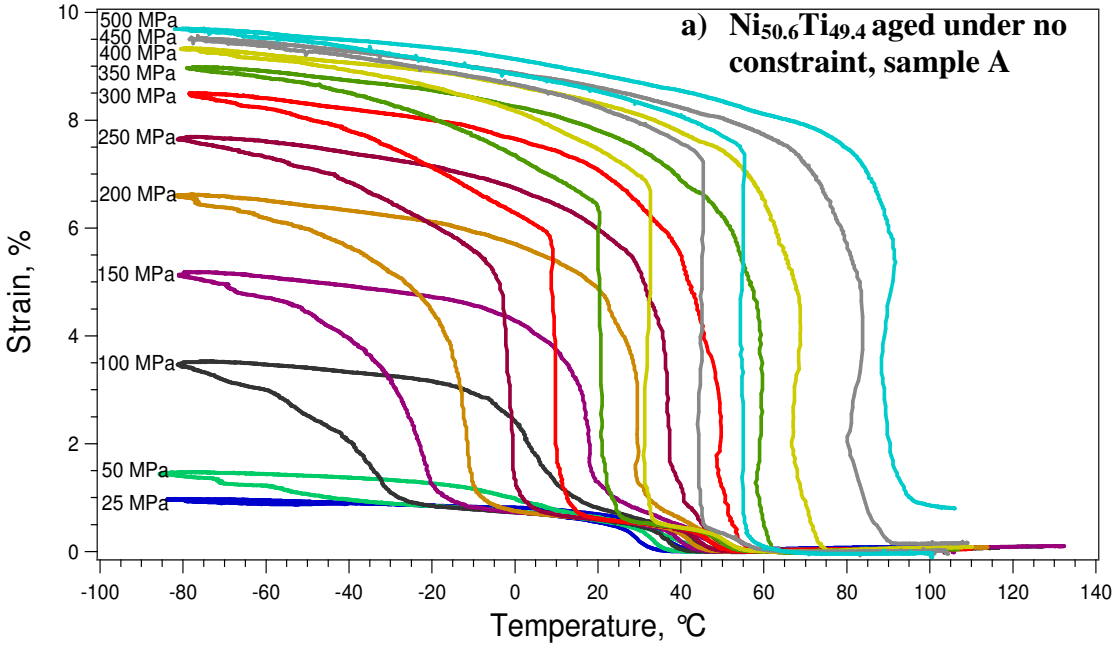

Figure 5. Isobaric thermal cycling experimental results for the single crystalline $Ni_{50.6}Ti_{49.4}$ samples aged under a) no constraint, b) tension, and c) compression.

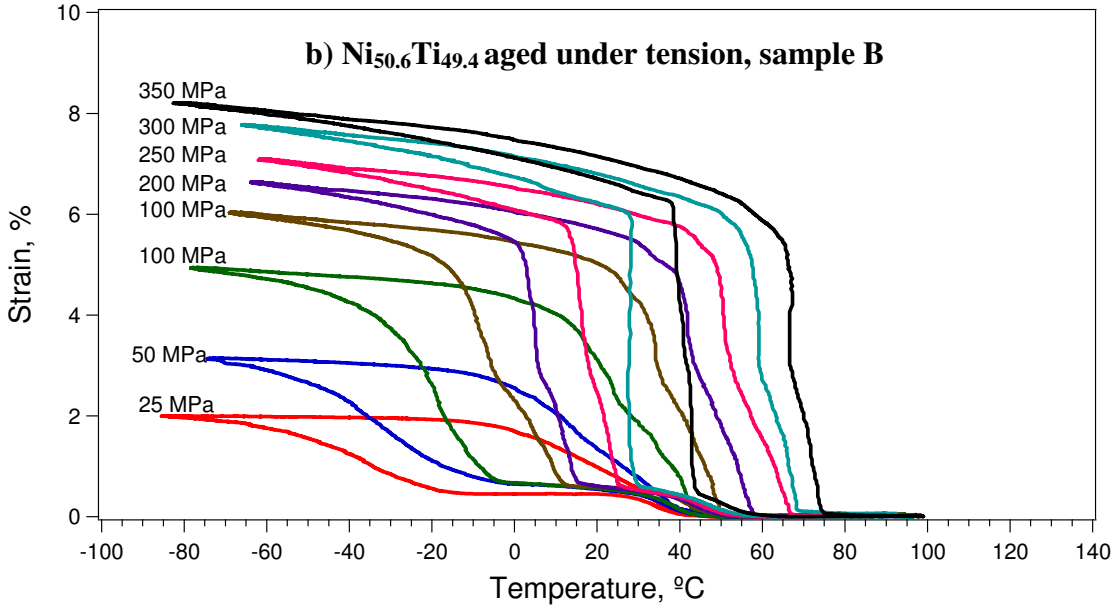

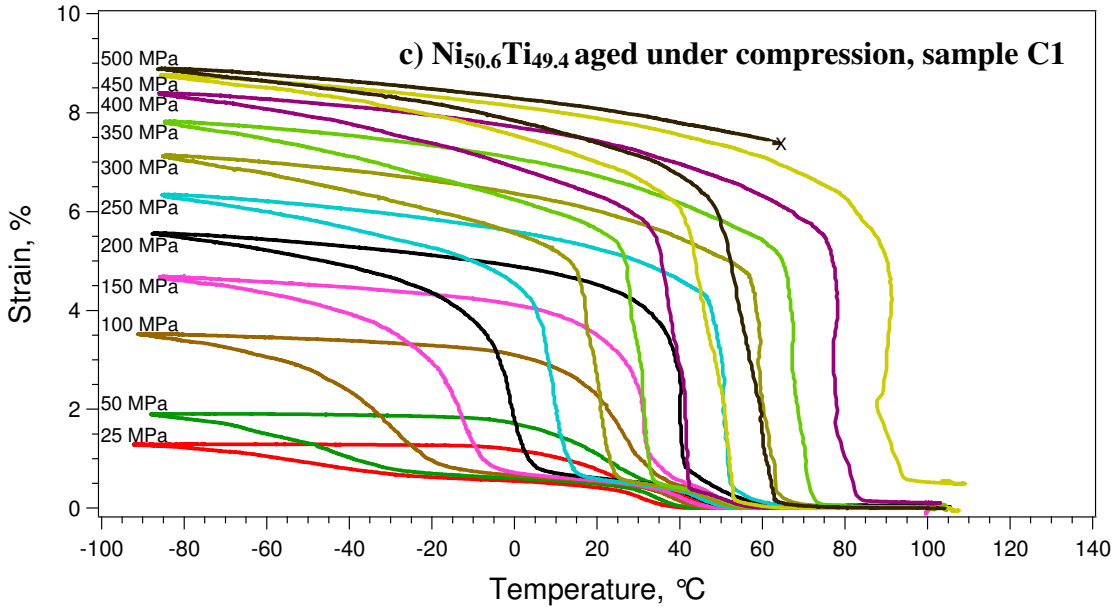

Figure 5. Continued

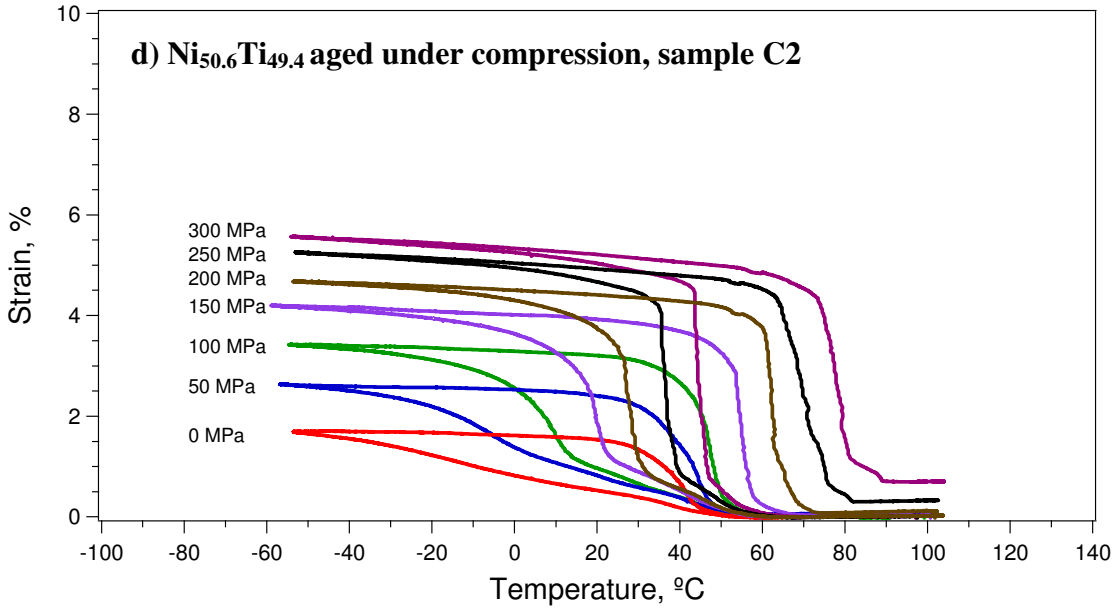

Figure 5. Continued

In each sample, the extent of the B2 austenite to B19' martensite transformation decreased as the applied stress increased for all samples. The extent of the B2 austenite to B19' martensite transformation is associated with the material's stored energy [8]. At higher stress levels, the transformation was virtually instantaneous, occurring at approximately the same temperature, before continuing with a secondary transformation.

There appears to be two distinct types of transformations occurring during the B19' martensitic transformation. At low temperatures, $T<M_f$, transformation occurs at increasingly smaller strain rates. This can possibly be attributed to a continuing transformation of regions left untransformed due to precipitate location and inhomogeneous microstructure. Since regions immediately surrounding the precipitates

are more highly stressed and likely have a lower Ni content, the first transformation could consist of this area followed by a subsequent transformation of the regions unstressed by the precipitates. This occurrence was shown by Khalil-Allafi *et al*. through TEM investigation of temperature dependent transformation characteristics. Khalil-Allafi noticed that the R-phase nucleates around precipitates. Upon completion of the B19' martensite transformation, R-phase still remains. The remnant R-phase began to transform to B19' martensite only after decreasing the temperature further [21]. A second potential reason could be the detwinning of martensite in the absence of a solid-to-solid phase transformation [3].

The results of the isobaric thermal cycling experiments show that a temperature decrease occurred during the back transformation to austenite. The temperature decrease occurred after differing stress levels dependent upon the sample aging history. This is especially noticeable at the 450 MPa and 500 MPa stress levels in Figure 5. This temperature decrease appears to correspond to the non-distinct regions of the R-phase as shown in the figures. In other words, above certain stress levels, the reverse transformation occurs as a single stage B19' to B2 austenite transformation instead of B19' to R-phase to B2 transformation. Distinct R-phase refers to stress levels of the isobaric thermal cycling experiments where the R-phase hysteresis either decreased or remained constant. This is consistent with 300 MPa, 200 MPa, 50 MPa, and 100 MPa for samples A, B, C1, and C2 respectively, as shown in Figure 6. Since the martensite to austenite transformation is an endothermic process, upon transformation, additional

energy is spent during the reverse transformation causing a reduction in the specimen temperature. The degree of energy release is correlated to the amount of material transforming, therefore, the more stress that is applied, the larger the energy release will be. This is consistent with the results of the isobaric thermal cycling experiments.

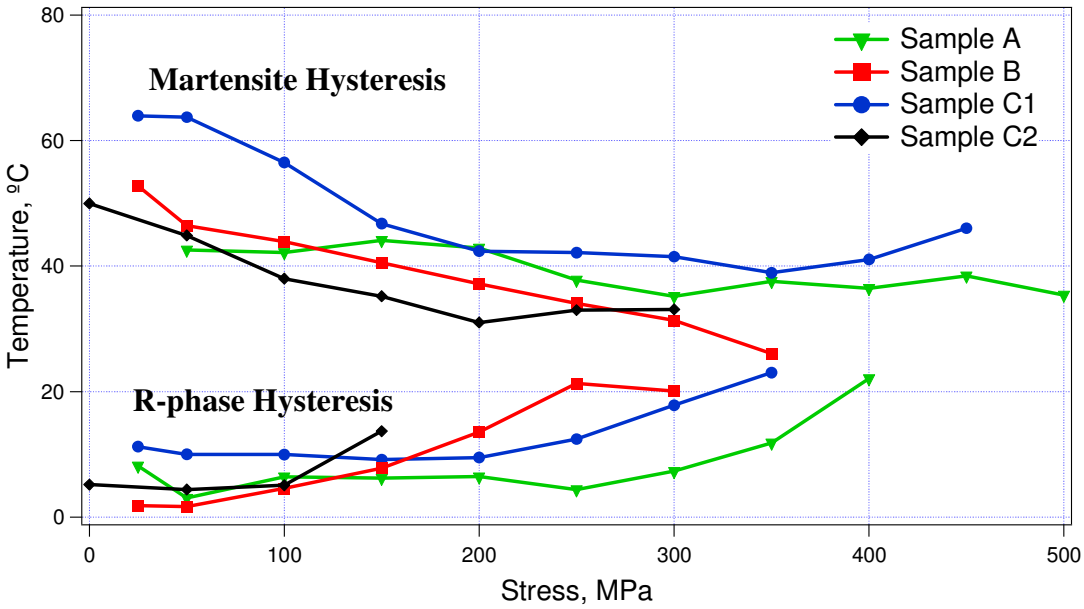

Figure 6. Resulting R-phase and martensite temperature hysteresis response from the isobaric thermal cycling experiments for the $Ni_{50.6}Ti_{49.4}$ single crystalline samples.

Figure 7 shows the strain-temperature results from the isobaric load bias experiments for each single crystalline sample under zero applied stress. Samples B and C were expected to show TWSME, while sample A was not. Only sample C2 showed TWSME, while samples A, B and C1 each underwent dissimilar transformations indicative of limited TWSME. The samples displayed different transformation behaviors and produced varying transformation strains.

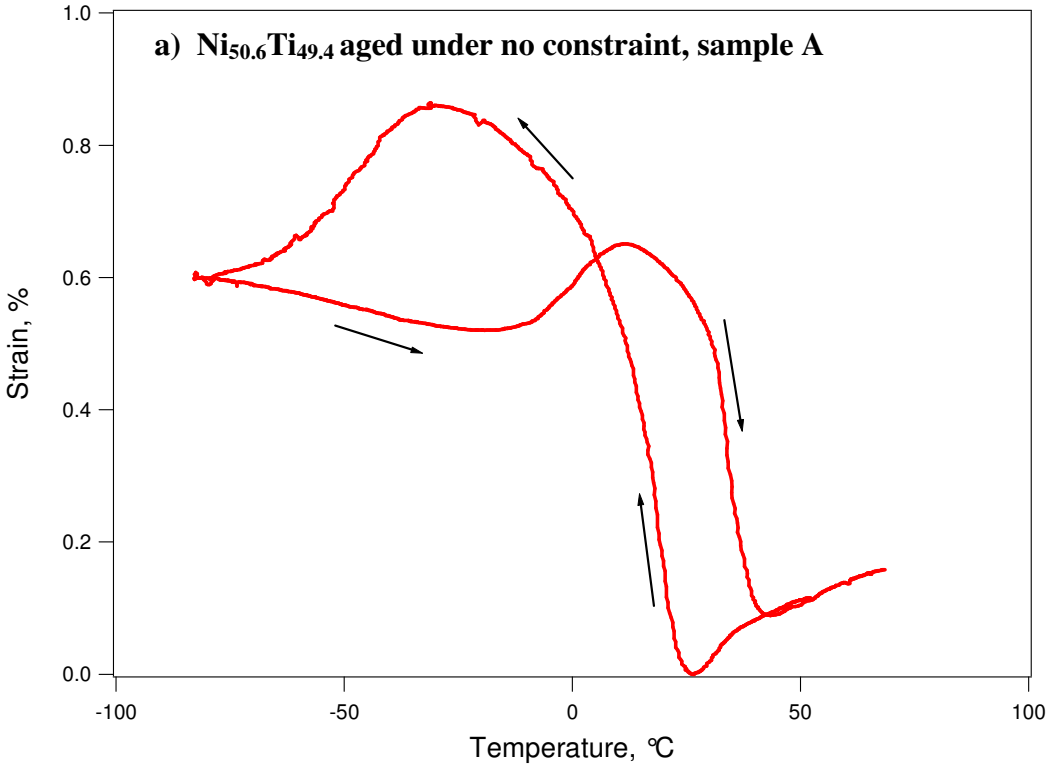

Figure 7. Strain-temperature curve response from the isobaric load bias experiments for $Ni_{50.6}Ti_{49.4}$ single crystal samples under 0 MPa. a) aged under no constraint, b) aged under tensile stress, c) aged under compressive stress: sample C1, and d) aged under compressive stress: sample C2.

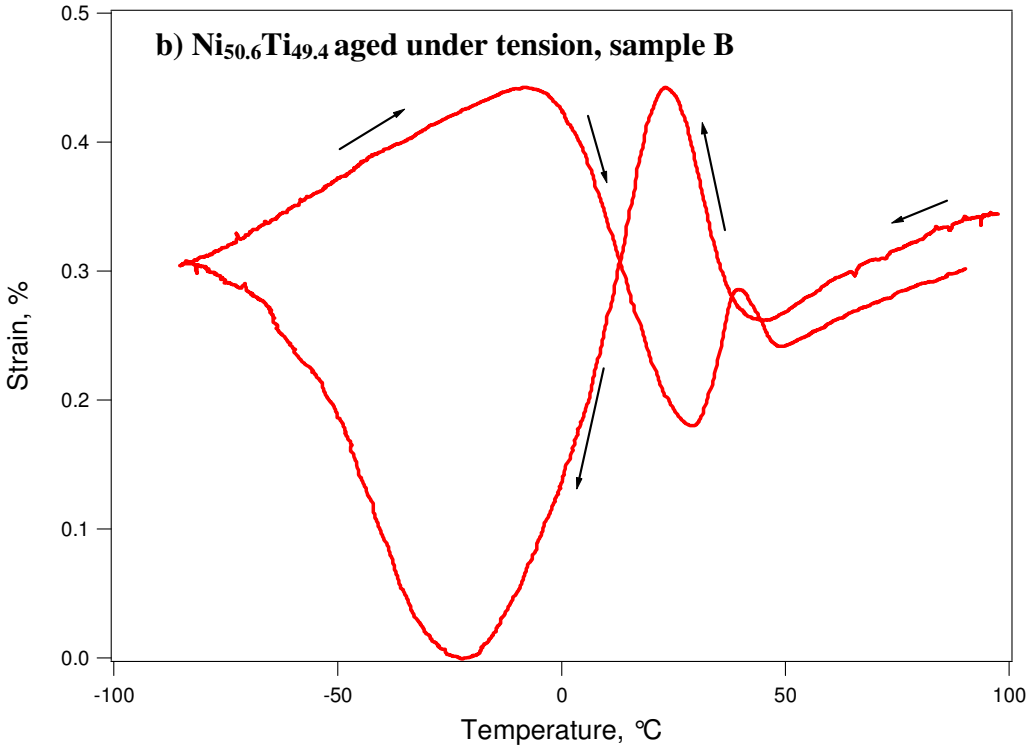

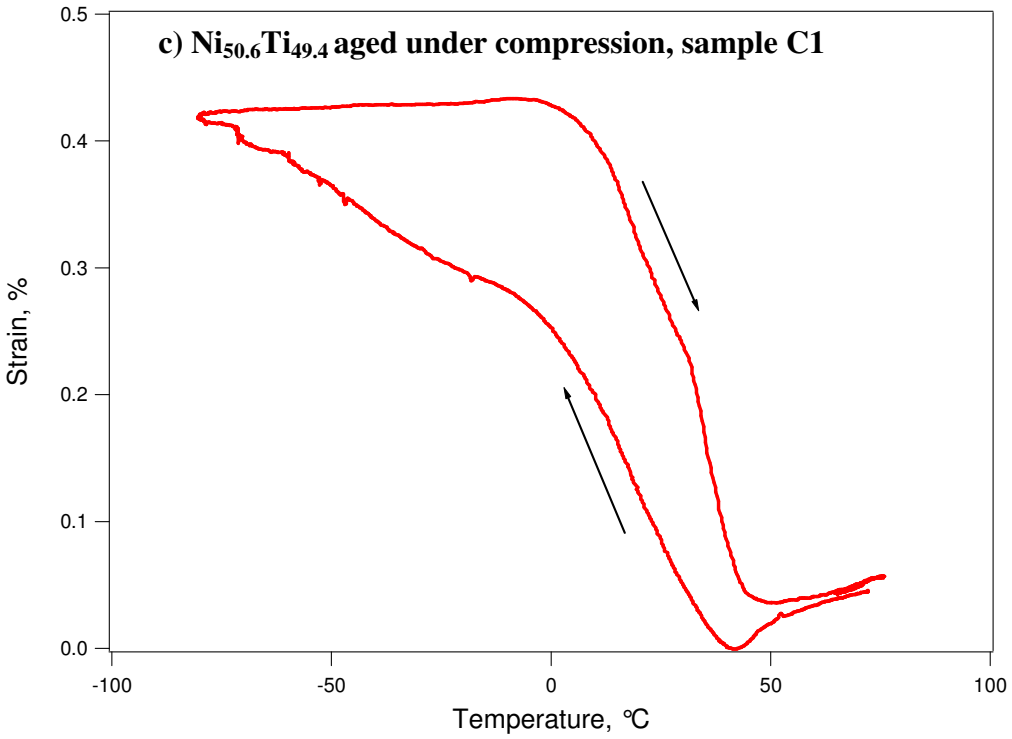

Figure 7. Continued

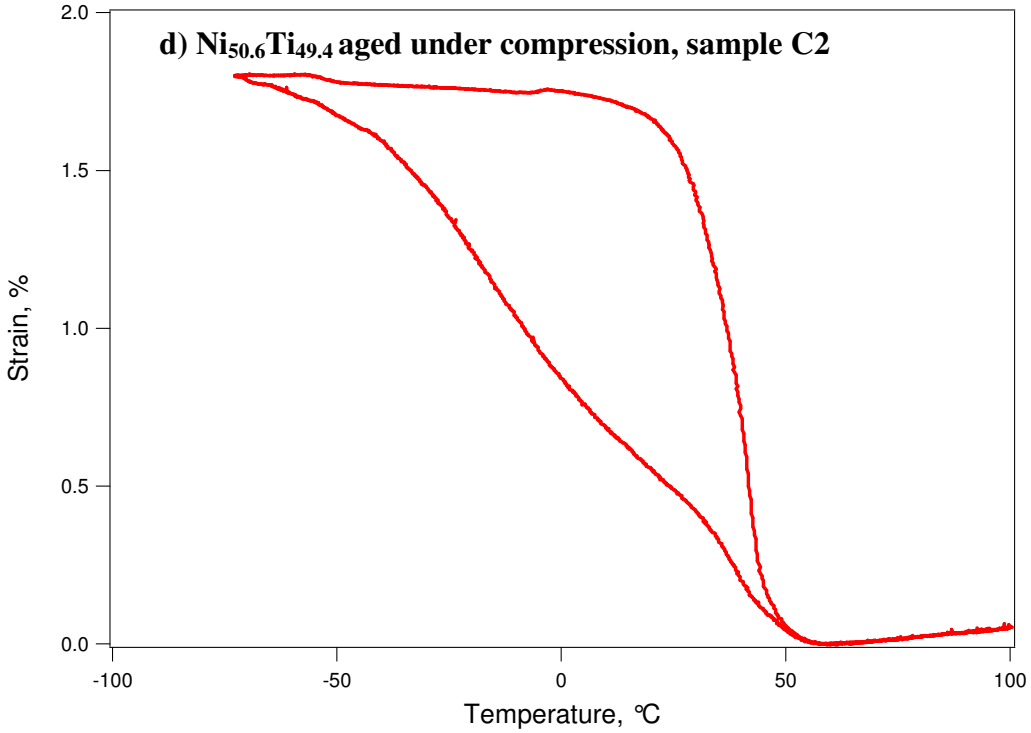

Figure 7. Continued

Sample C2 produced a 1.7% total TWSME strain and 0% irrecoverable strain. The strain continuously increased once transformation began during cooling, and continuously decreased during heating. The sample completely transformed to R-phase, however, did not completely transformed to the B19' martensite phase because the M_f was below the cooling capabilities of the isobaric thermal cycling setup. During the reverse transformation the sample appears to have transformed directly from the B19' martensite phase, with remnants of R-phase, to the B2 austenite phase.

Sample A initially underwent a 0.83% transformation strain followed by a 0.13% strain decrease during cooling. Throughout the heating of sample A, the strain initially

decreased slightly followed by a slight increase for a net change of approximately +0.06% change followed by the subsequent 0.56% strain decrease leading to complete recovery of the shape change during cooling.

Sample B initially underwent a positive strain transformation of approximately 0.2% in magnitude. Upon further cooling the sample exhibited a -0.41% transformation strain followed by a +0.3% transformation strain. At the start of heating, the sample continued to increase in strain by 0.11%. At the end of the heating cycle the shape change is over recovered by approximately 0.39% strain.

Sample C1 continuously increased in strain during cooling, and decreased during heating. The sample appears to have underwent two separate transformations in the forward transformation because the strain rate changed abruptly at approximately 0°C. Upon heating, the sample again appears to exhibit two transformations with a change in strain rate occurring at 39°C. In all, the sample achieved a 0.41% transformation strain, however, did not completely recover as there was a 0.1% irrecoverable strain.

While samples C1 and C2 appear to have produced dissimilar results, each underwent a continuous tensile strain transformation in the forward transformation and a continuous compressive strain transformation in the reverse transformation. The different results could have been caused by compositional discrepancies between the samples themselves which would indeed cause the differing results. Even a 0.3at% Ni change can cause TWSME to disappear as shown by Nishida *et al*. [6]

Figure 8 shows the stress versus temperature phase diagrams for each of the single crystalline samples. The start temperature of each sample's transformation varied with sample A having the lowest temperature and sample B having the highest. This is the same behavioral pattern shown by the martensite start temperatures, M_s. Miyazaki *et al.* determined using the electrical resistance method that the M_f, M_s, A_s, and A_f temperatures of a $Ni_{50.6}Ti_{49.4}$ sample were -145°C, -83°C, -85°C, and -52°C, respectively. That particular sample was swaged and then drawn at room temperature followed by a 1000°C solution heat treatment. [22] An increase in the transformation temperatures was expected due to aging.

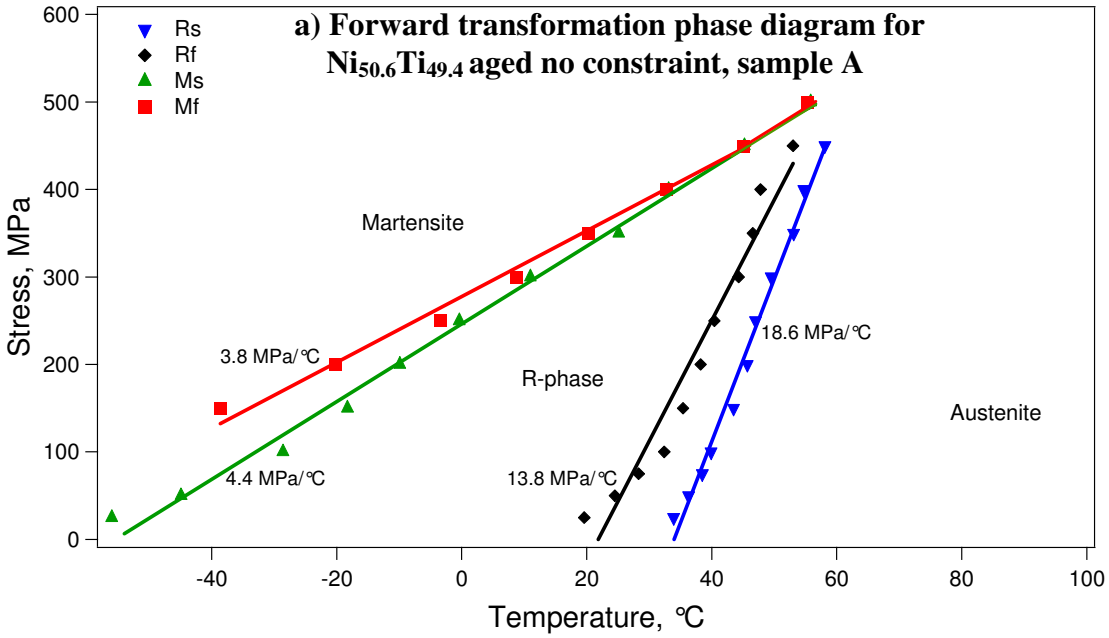

Figure 8. Stress vs. temperature phase diagram of $Ni_{50.6}Ti_{49.4}$ single crystal along the [112] orientation. a) sample A forward transformation, b) sample A reverse transformation, c) sample B forward transformation, d) sample B reverse transformation, e) sample C1 forward transformation, f) sample C1 reverse transformation, g) sample C2 forward transformation, and h) sample C2 reverse transformation.

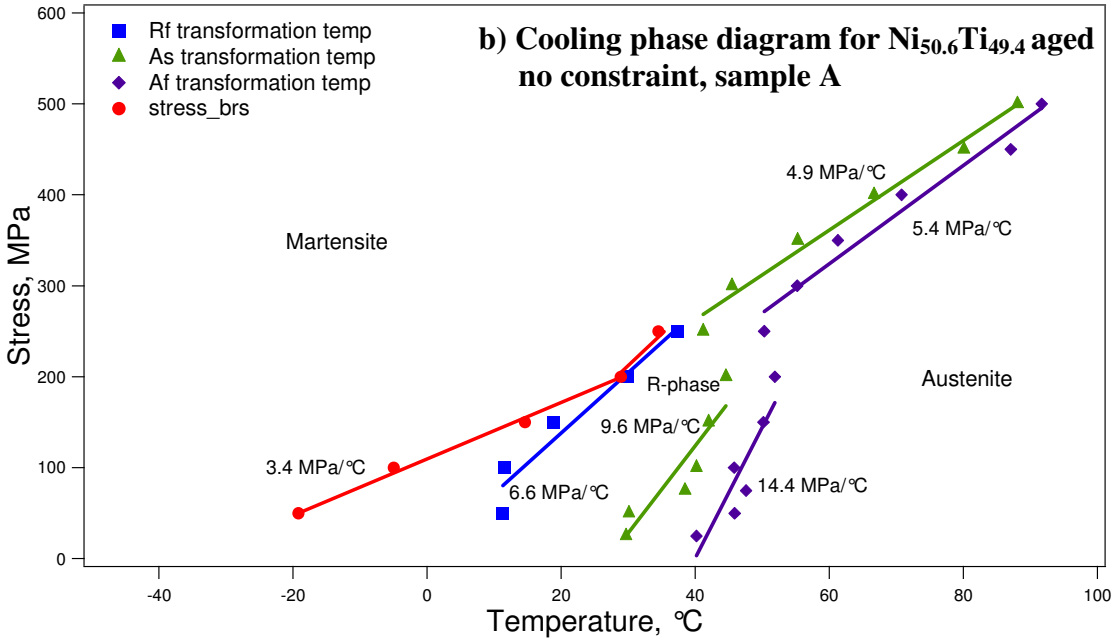

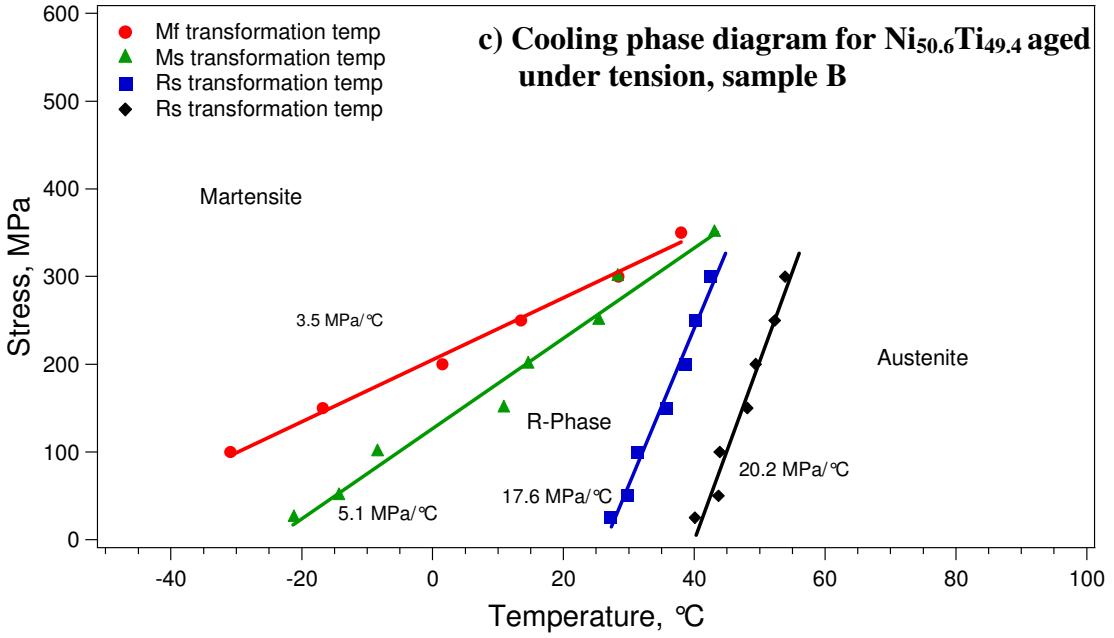

Figure 8 Continued

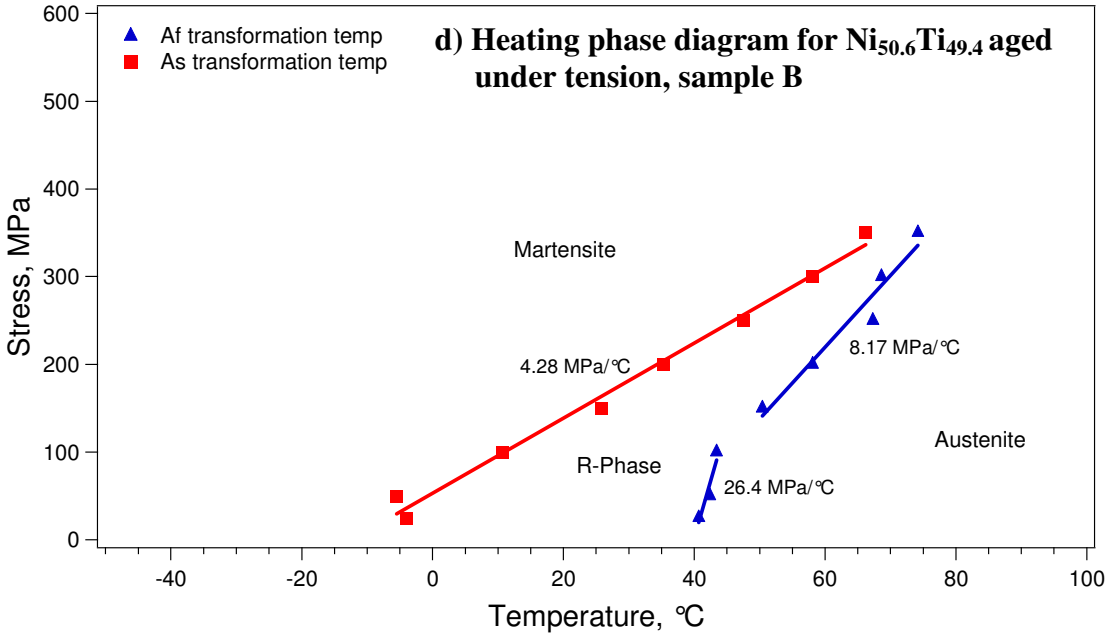

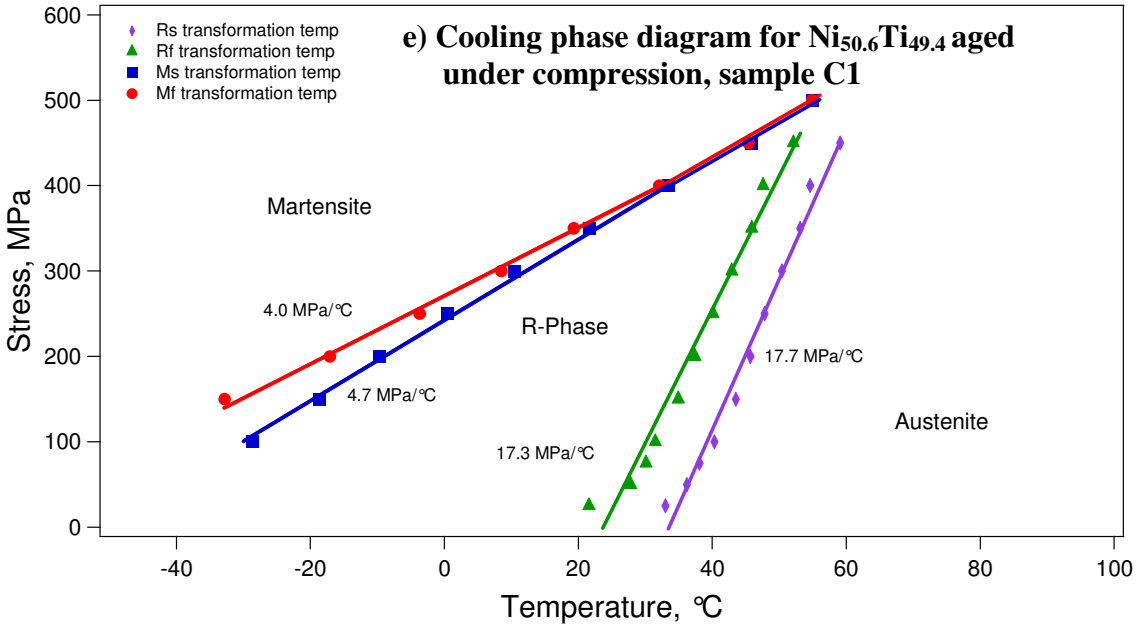

Figure 8. Continued

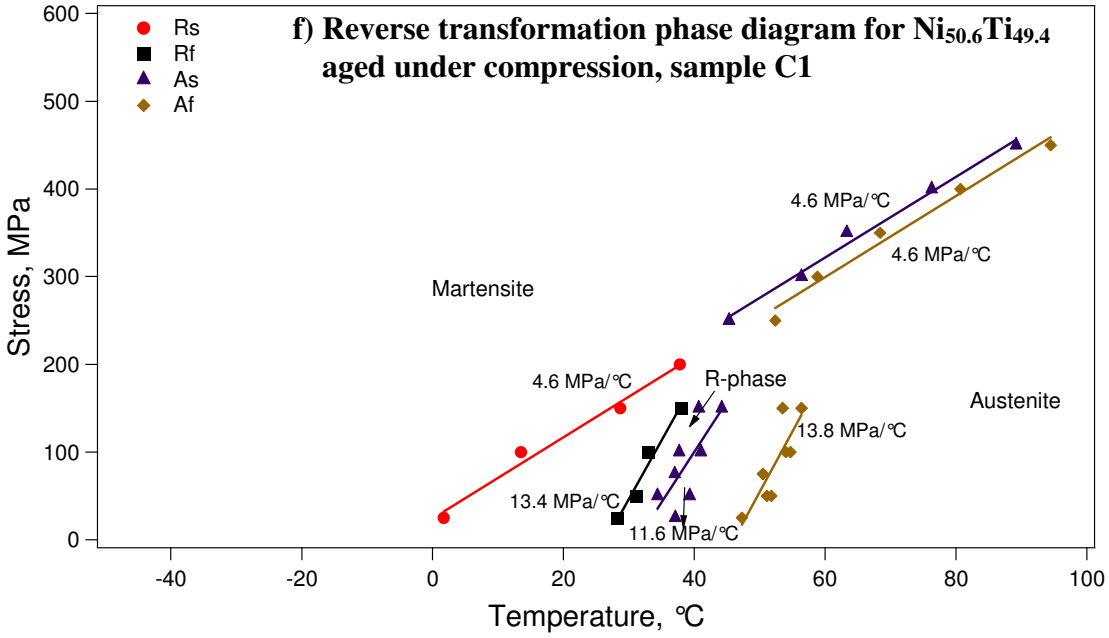

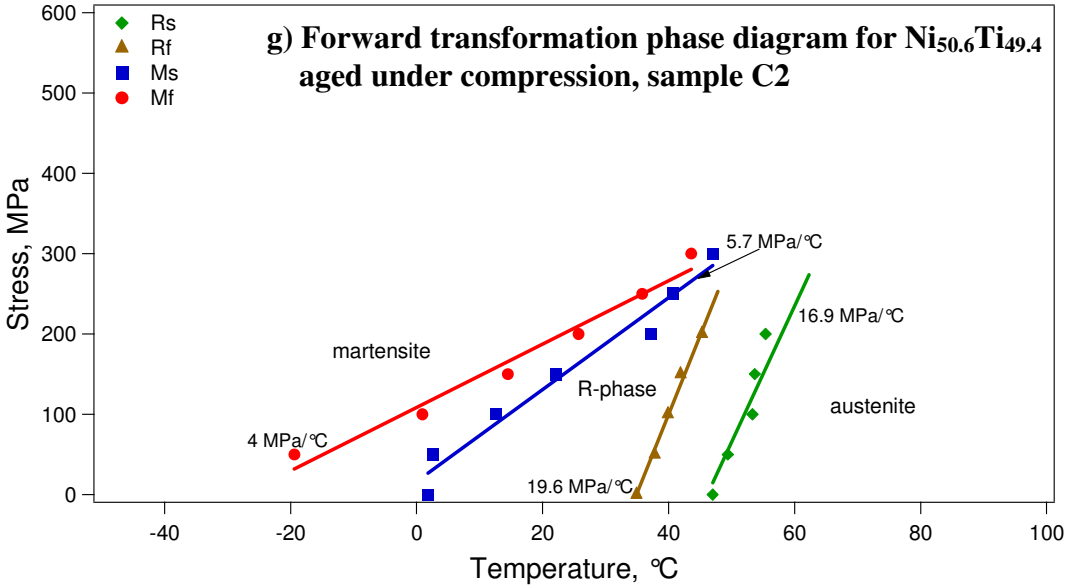

Figure 8. Continued

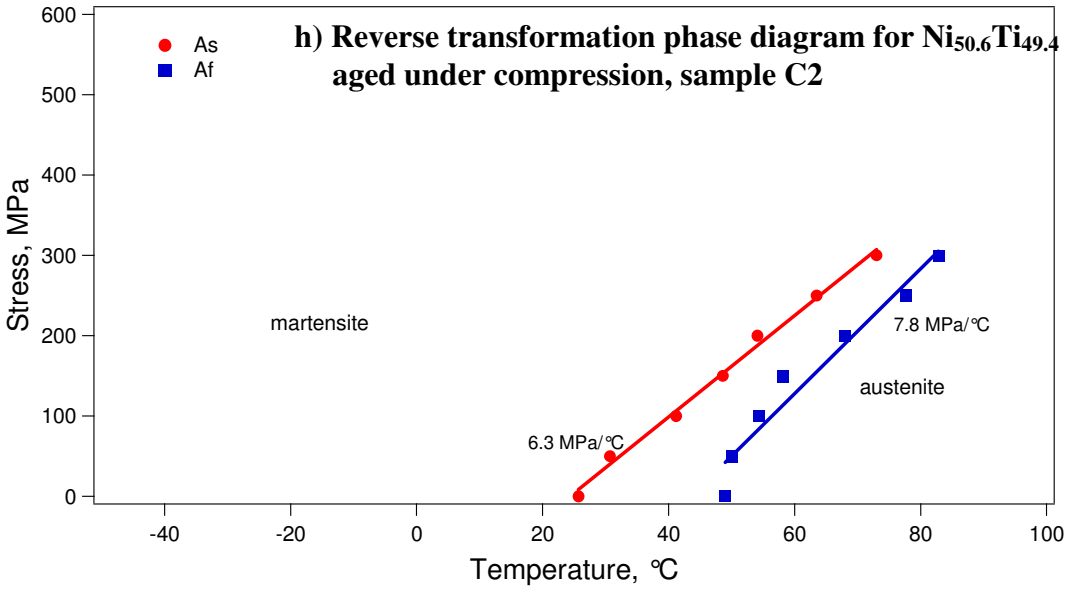

Figure 8. Continued.

According to Ren, aging temperature largely affects the R-phase transformation start temperature, R_s, while aging time and alloy composition minimally affect R_s. [2] The R_s for individual stress levels was relatively constant between samples A, B, and C1, with a maximum standard deviation of 3.8°C. However, when C2 was factored in, the maximum standard of deviation increased by a factor of approximately 2 to about 6.3°C. Therefore, it appears that sample C2 was likely aged at a different temperature and the aging stress type and orientation minimally affect R_s.

In regards to the R-phase formation in Figure 7, while samples A and B exhibited multiple strain expansions and contractions, all the samples initially produced tensile strain transformation. This appears to be consistent with the R-phase formation. Possibly to some degree, the R-phase was successfully biased to induce the R-phase

transformation, although the B19' variants were unsuccessfully biased in samples A, B, and C1.

Figure 9 a and b show the temperature-strain response for each of the $Ni_{50.6}Ti_{49.4}$ single crystalline samples at 100 MPa and 300 MPa respectively. From the figure we clearly see the varying transformation and irrecoverable strains, hystereses, and transformation temperatures. In Figure 9a, it is clear that sample C2 had higher transformation strains than the rest of the samples. Sample C2 also had a comparable, but slightly smaller, total transformaton strain when compared with sample C2. At 100 MPa, sample B produced a noticalbly higher transformation strain when compared with each of the other samples. This difference is likely due to the precipate morphology activation of a specific martensite variant that yeilds a higher martensitic transformation strain. At 100 MPa, none of the samples produced any irrecoverable strain. At 300 MPa, the transformaton strain of sample C2 decreased noticably when compared with each of the other samples. Additionally the transformation temperatures for sample C2 are higher than the other samples. The strain associated with the secondary transformation that occurs at temperatures lower than M_f is much lower for sample C2 than each of the other samples. Samples A, B, and C1 also show no signs of irrecoverable strain, whereas, sample C2 shows a noticable irrecoverable strain. Sample A produced the highest martensitic transformation strain.

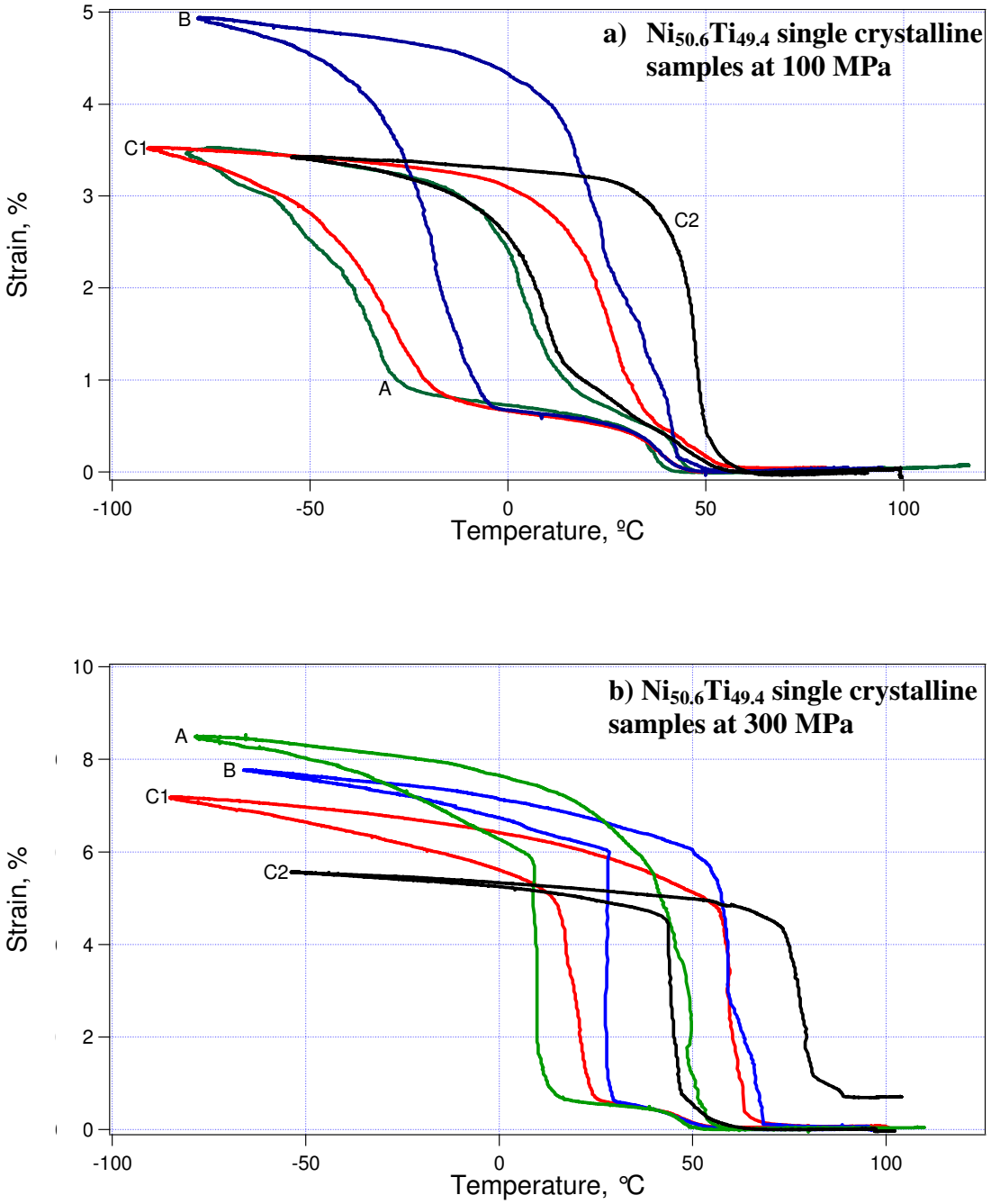

Figure 9. Strain-temperature response for the $Ni_{50.6}Ti_{49.4}$ single crystalline samples at a) 100 MPa and b) 300 MPa.

Figure 10a shows that as stress was applied to each sample, regardless of the aging history, the austenite, R-phase, and martensite transformation temperatures increased. Each sample underwent different transformation strains at each applied stress level. This can be attributed to the varying precipitate morphology of each sample. The transformation strains increased with increasing applied stress but did not saturate.

The irrecoverable strain associated with each sample's isobaric thermal cycling experimental results is plotted in Figure 10b. From Figure 5, it is clear that the onset of irrecoverable strain is connected to the disappearance of the R-phase. The critical stress level, stress level at which slip occurs, is approximately 400 MPa for both samples A and C1. It was not possible to determine the critical stress level for sample B due to the incomplete experimental results. In a study by Ishida and Miyazaki, it was found that a Ti-51.3at%Ni thin film sample aged at 400°C for 1 hr produced a similar critical slip value that was found in this study, for samples A, B, and C1. [23] The Ishida and Miyazaki sample displayed the same R-phase irrecoverable strain trend that was found in the present study. Although it is uncertain as to exactly why the disappearance of R-phase coincides with the onset of irrecoverable strain, Ishida and Miyazaki found that there is an empirical relationship between the precipitate size of aged Ni-rich NiTi SMAs and the critical slip level. If the R-phase disappears at stress values greater than the critical stress level then perhaps the R-phase disappearance is also correlated to the precipitate size in aged Ni-rich NiTi SMAs.

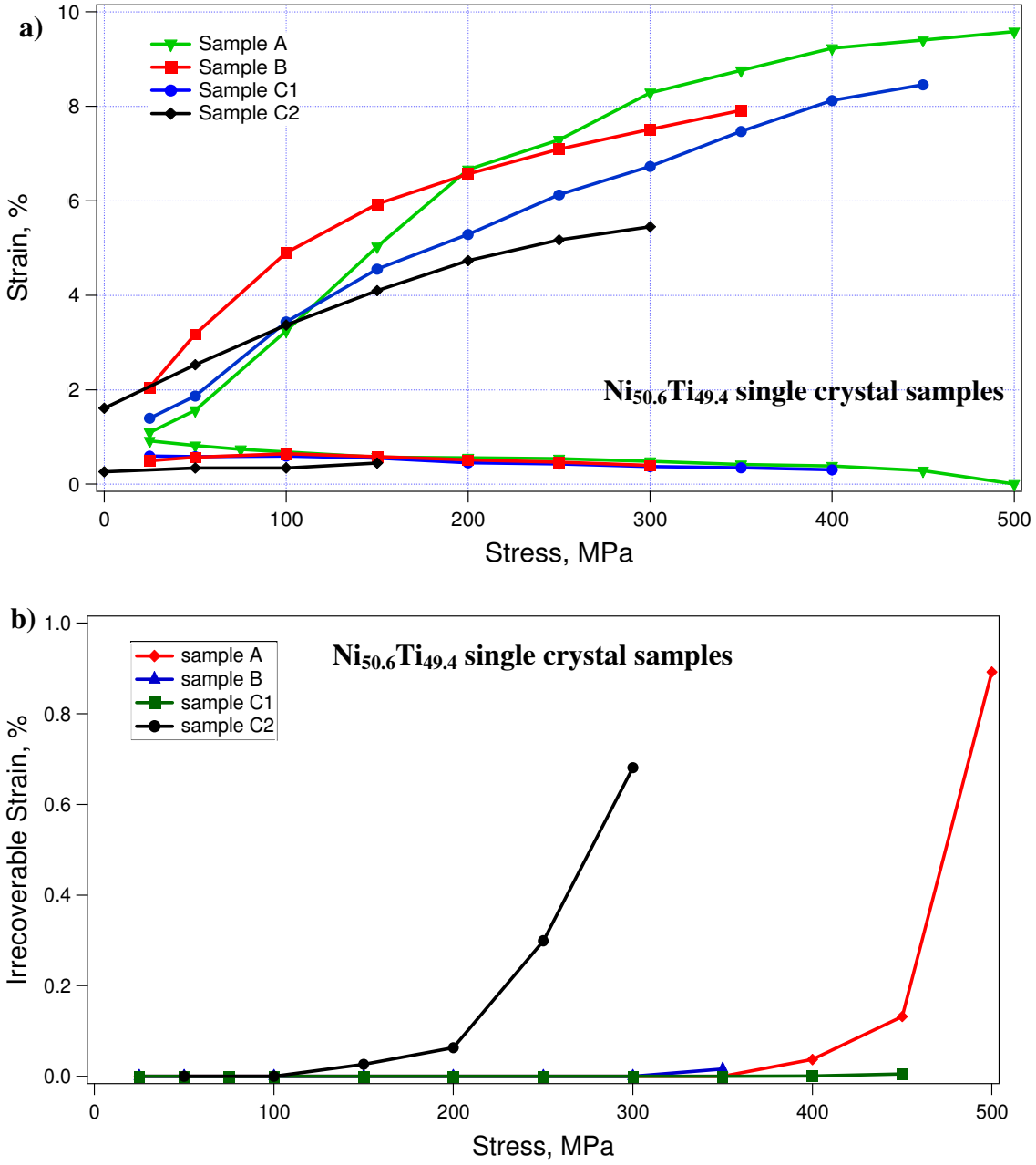

Figure 10. Resulting a) R-phase transformation, total transformation and b) irrecoverable strains from the $Ni_{50.6}Ti_{49.4}$ single crystal samples from the isobaric thermal cycling experiments.

Lattice invariant shears could also explain the R-phase–irrecoverable strain trend. Zhang *et al*., using the energy minimization theory, showed that only 4 twin types qualify as lattice invariant shears in the single step transformation (austenite→martensite) whereas in the 2 step transformation (austenite→R-phase→martensite), 8 twin types qualify. Lattice invariant shears can possibly be used to describe strain recoverability behavior in Ni-rich NiTi SMAs. [24] According to Otsuka and Ren, the precipitates add energy to the NiTi matrix, that in turn affects the stability of the R-phase and Martensite. Martensite is more easily affected than the R-phase by precipitates. This is what allows the R-phase to serve as the transformation path of minimum energy. [2]

Sample C2 displayed a different dimensional stability, R-phase and total transformation behavior as compared to samples A, B, and C1. The R-phase transformation strain appeared to increase with increasing applied external strain. Also, upon completion of the R-phase transformation, there was a continued transformation at a smaller strain rate. Also, the total transformation strain of sample C2 was higher that of samples A and C1 at stress levels below 100 MPa, after which the sample displayed the lowest total transformation strain of all the samples, Figure 10a. It is worth noting that sample C2 was cooled to approximately -60°C.

The onset of irrecoverable strain, in sample C2, occurred at a lower stress level than the other samples, approximately 100 MPa. This is shown in Figure 10b. Although the only

reported developmental difference stems from the sample orientation, [-112] instead of [112], there appear be other differences although it is not certain where these may come from. Possibilities include sample composition, and/or aging temperature or time.

Superelasticity Experimental Results and Analysis

Figure 11 shows the stress-strain response of the superelasticity test performed at 50°C for sample A. The stress-strain response can be divided into four stages. During stage I, elastic deformation occurs. In this region, the sample remains in the austenite phase. During stage II the nucleation and propagation of stress induced martensite occurs. The sample, at a relatively constant stress, appears to undergo a Lüders like deformation. During stage III martensite deforms elastically. While the SMA matrix microstructurally is a single crystal and precipitates themselves do not transform, they can often hinder the transformation of the matrix immediately surrounding the precipitates. Therefore, during stage III, pockets of austenite previously left untransformed due to their relative location to the precipitates may continue to transform to stress induced martensite. This is comparable to Tan *et al*. findings that show that non-transformable inclusions can isolate areas of austenite thereby requiring more stress to induce a martensitic transformation [25]. During stage IV appreciable irrecoverable strain occurred due to the plastic deformation of martensite. This region is also known as the second plateau region. [26]

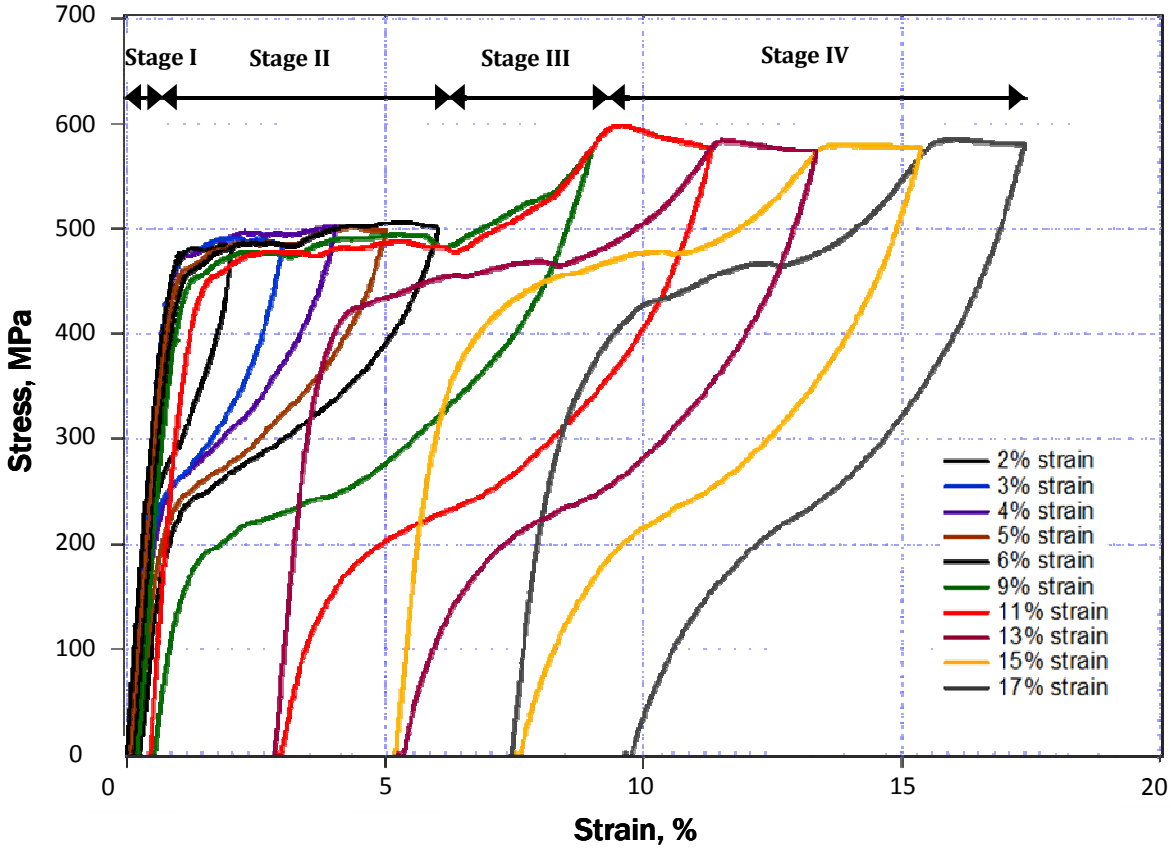

Figure 11. Sample A, aged under no constraint, single crystal $Ni_{50.6}Ti_{49.4}$ stretched at incremental strains up to 17% at 50°C.

Table 3 shows the strain produced in the stage IV region and the irrecoverable strain experienced by the sample at different experimental strain levels during the 50°C superelasticity experiment. Clearly, there is a direct correlation between how much additional plastic strain was applied and how much irrecoverable strain was observed. This indicates that the plastic deformation in martensite occurs very locally, and that plasticity does not affect the back transformation to austenite in other regions of the sample, but influences only the back transformation of that particular plastically

deformed region. This behavior has not been reported before in any SMA. The reason for such a unique behavior will be explained with the help of TEM images.

Table 3. During stage IV of the 50°C superelasticity test, sample A began to experience significant irrecoverable strain. The table shows the associated irrecoverable strain and inelastic strain associated with martensitic slip that occurs in the second plateau region.

strain (%)	Stage IV strain (%)	Irrecoverable strain (%)
11	1.93	2.55
13	1.83	2.48
15	1.8	2.42
17	1.64	2.33

In Figure 11, the sample appears to remember the deformation experienced by previous experimental cycles. The deformation memory is manifested differently in stages II and IV. In stage II, the deformation memory is shown by the appearance of reductions in the stress levels up to the strain level that the previous loading cycle was interrupted at. Additionally, indentations occur at the strain levels at which the previous loading cycle was interrupted. In stage IV, the material shows a decreased flow stress until the sample reaches the level of deformation from previous experimental strain cycles. Duerig suggests that the deformation memory is caused by either the formation of dislocation networks that guide the formation of internal stresses. The second theory is that martensite embryos are left behind after superelasticity recovery that act like "seeds" encouraging the same martensite variants to form during subsequent

superelasticity cycles. [27] This second theory seems plausible after looking at a set of TEM and OM images taken upon fracture of the sample during the superelasticity experiments.

The OM and TEM images in Figure 12 and Figure 13 show [112] and [114] twins in austenite. The images themselves were taken at room temperature. Theoretically, [112] twins in austenite are impossible to form since dislocations associated with twinning have to destroy the order in B2 austenite to be able to form these twins. [28] Considering the unusual response upon loading and unloading in stage IV as summarized in Table 3, we believe that these twins in austenite are a consequence of deformation twins (also known as compound twins) in martensite. Our hypothesis is that plastic deformation in Stage IV is due to mainly to compound twins in martensite.

Since the material is very strong due to precipitates, we believe that negligible dislocation slip accompanies the twin formation. The twins are quite small (on the order of 200 nm and below in thickness) and due to very small precipitates, there is an elastic energy storage even though these compound twins form, as evidenced by the significant superelasticity even after 17% applied strain. Therefore, upon unloading, these compound twins transform back to austenite as twins in austenite instead of as single crystal of austenite. For this theory to be true, from lattice correspondence between austenite and martensite, the twins, in martensite, corresponding to [112] and [114] twins of austenite must be compound twins. [114] austenite twins correspond to [201] twins in

martensite. Indeed, Nishida *et al*. demonstrated using in-situ TEM that [201] martensite twins transform to [114] twins in austenite upon heating. [112] austenite twins corresponds to [113] twins in martensite. [29] Ishida *et al*. reported [113] twins in Ni-rich NiTi SMAs in thin films in the second plateau region. [30] These support our argument on the transformation of twins in martensite to twins in austenite upon unloading. Such observation opens a new possibility of twinning induced grain boundary engineering in SMAs.

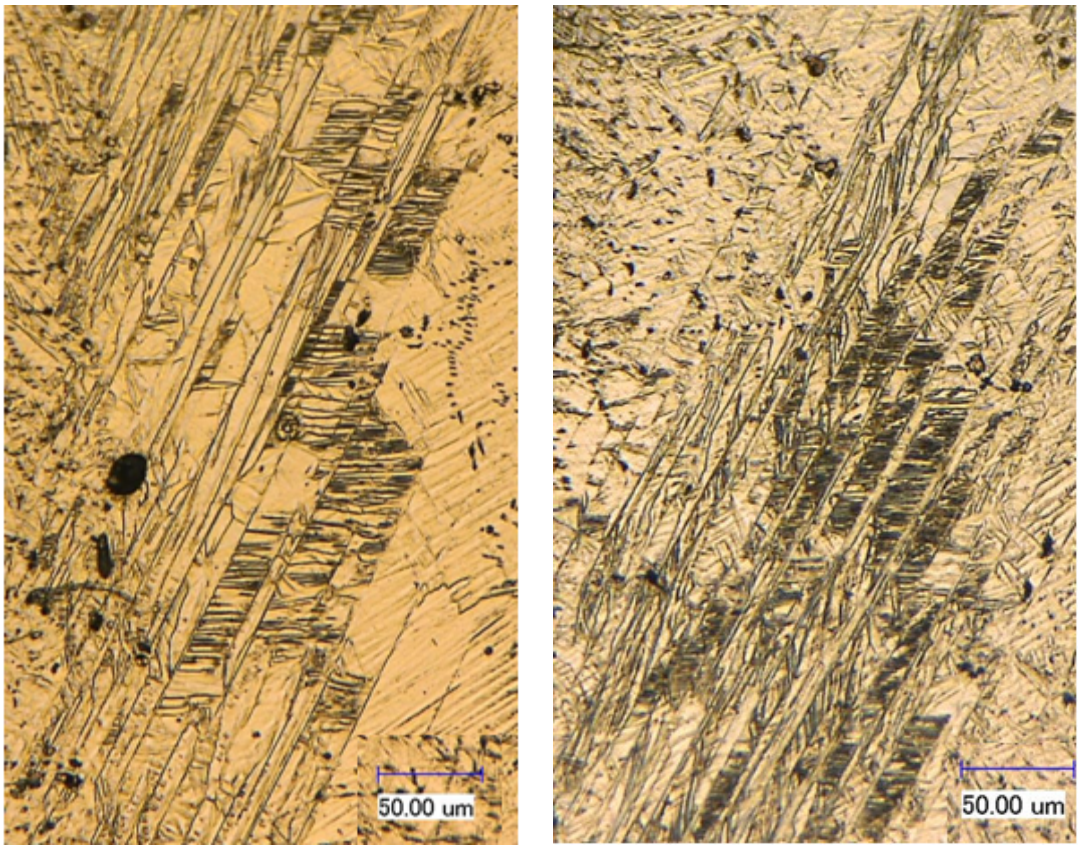

Figure 12. OM images of deformation twins produced during the superelasticity experiments. The images were taken at room temperature. The [112] direction is the horizontal direction.

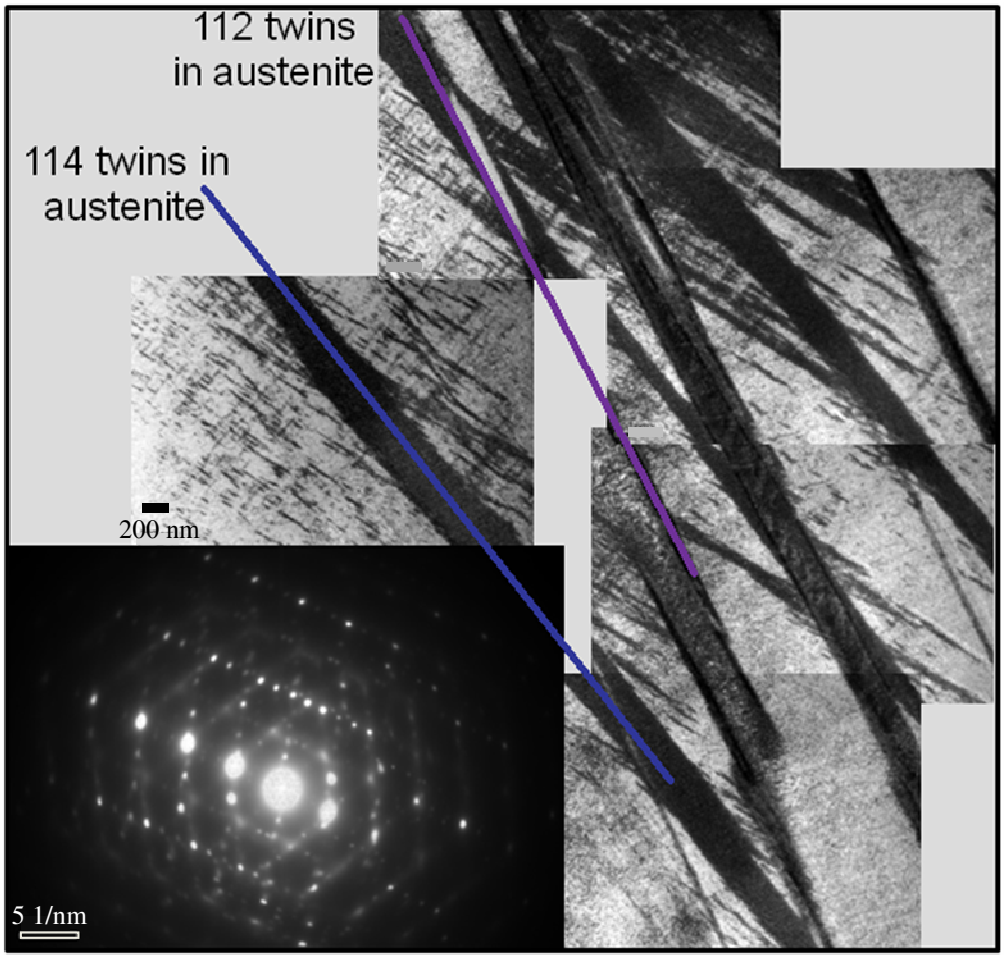

Figure 13. A compilation of TEM images of the deformation twins produced during the superelasticity experiments. The images were taken at room temperature in the B2 austenite structure with no B19' martensite present. The zone axis for the TEM image is [111]B2.

Figure 14 shows bright field TEM images of sample A and C1 with their corresponding diffraction patterns. The diffraction patterns show that precipitates are indeed present within the microstructure. It was not possible to distinguish the orientation of different precipitate variants due to the coherency stress field produced by the presence of the precipitates. However, the volume fraction of the precipitates are relatively significant.

From TEM images it was determined that the precipitates were approximately 30 nm or less in length.

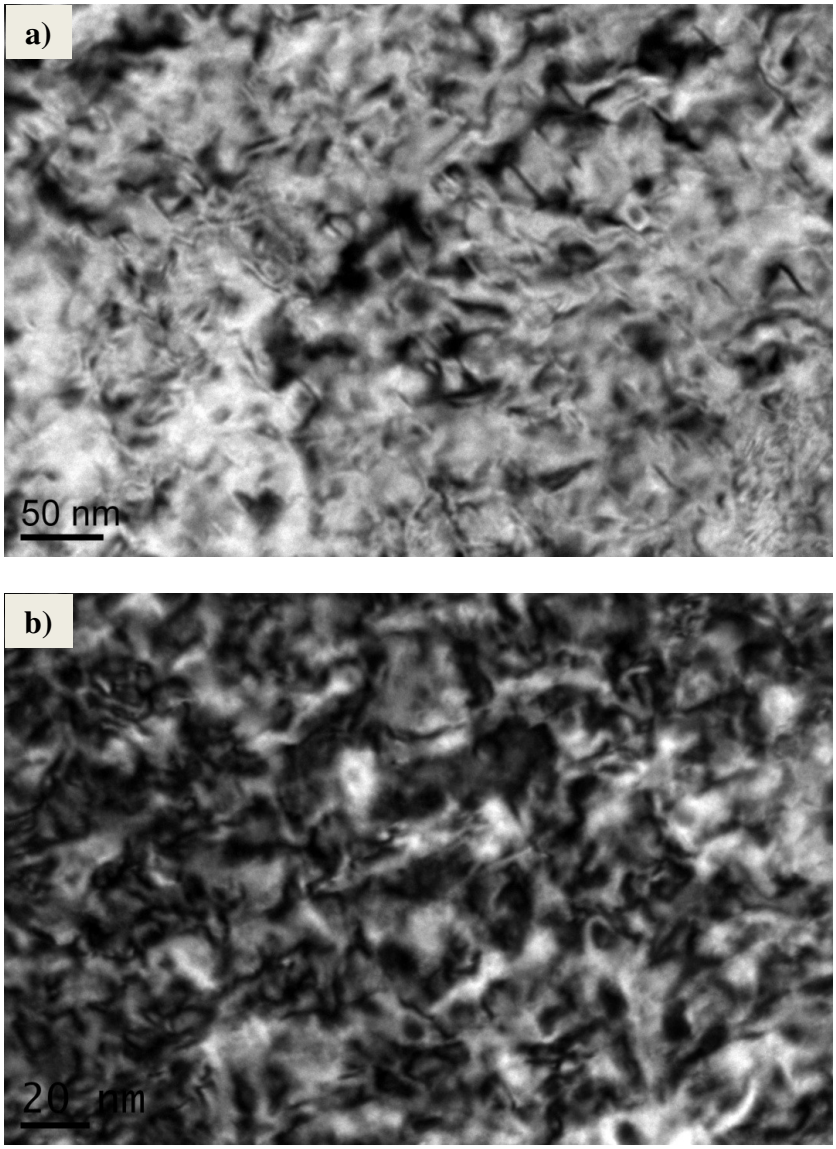

Figure 14. TEM images from a) sample A and b) sample B showing the coherency stresses produced by the presence of Ni_4Ti_3 precipitates. The images were taken at room temperature.

Figure 15 shows a bright field TEM image of sample B and the corresponding diffraction pattern. The figure shows aligned R-phase variants which mean that the microstructural morphology of sample B was able to at least in part bias R-phase martensite variants. Therefore, the initial 0.2% increase in strain, shown in Figure 7, is most likely the result of R-phase transformation.

The constrained aging of Ni-rich $Ni_{50.6}Ti_{49.4}$ single crystalline SMA samples lead to the appearance of TWSME in sample C2 that was aged under a 200 MPa compressive stress for 1.5 hours at 400°C after being homogenized at 1000°C for 1 hour. Mechanically this sample did not behave like the others as it showed irrecoverable strain at 100 MPa. Upon investigation of sample A, the sample that was aged under no constraint, through TEM analysis it was discovered that [112] and [114] twins were found in austenite as a result of plastic deformation during the superelasticity experiment. Since theoretically [112] and [114] twins cannot form in austenite, it is believed that [112] twins in austenite form as [113] twins in martensite, and [114] twins in austenite form as [201] twins in martensite.

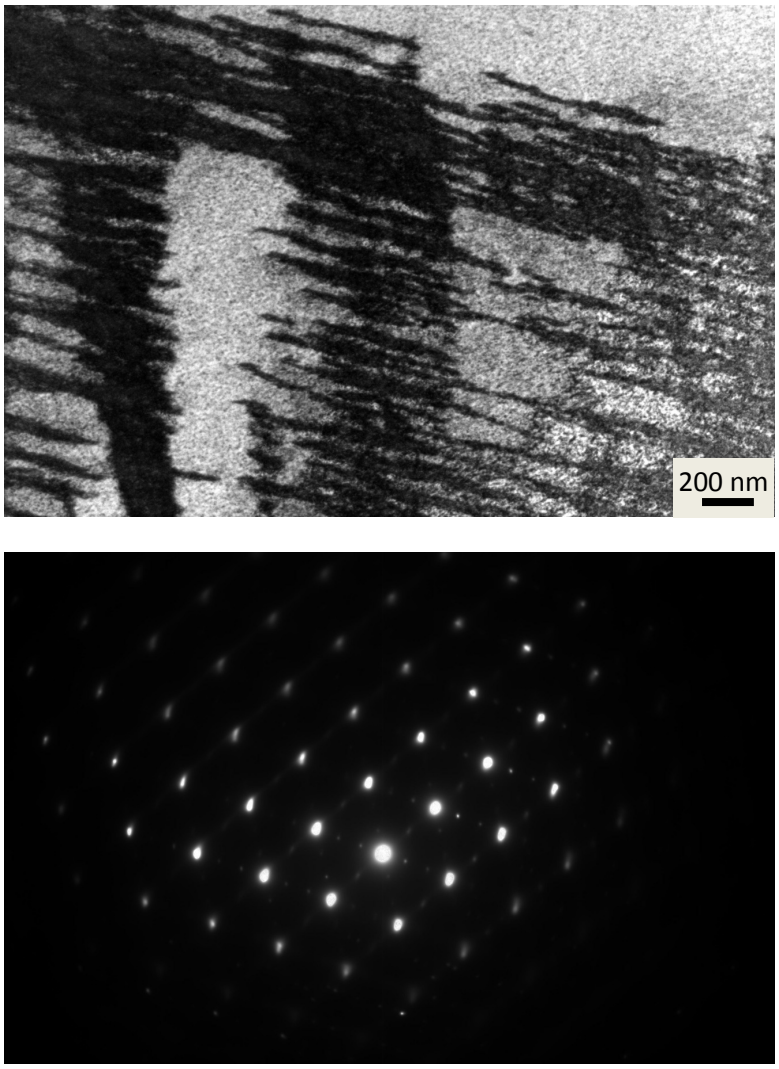

Figure 15. Bright field TEM image and corresponding diffraction pattern of sample B showing aligned R-phase variants. The image was taken at room temperature with a [111]B2 zone axis. The diffraction pattern also indicated the presence of precipitates.

CHAPTER IV

EFFECT OF AGING ON POLYCRYSTALLINE $Ni_{52}Ti_{48}$ SMAs

Isobaric Thermal Cycling Experimental Results and Analysis

Polycrystalline SMAs behave slightly different as compared to single crystalline SMAs. Grain boundaries affect martensitic transformations, transformation strain levels, the critical stress level, and behavior of precipitate formation. Each grain is not necessarily oriented along the same direction; therefore, not necessarily the same precipitant variant is biased within each individual grain when stress is applied during aging. It still is expected, however, that 4 precipitate variants will form when aging is performed free of any applied stress. Sample composition, has been found to affect the homogeneity of Ni_4Ti_3 precipitates within individual grains. [31,32] In the $Ni_{52}Ti_{48}$ polycrystalline SMAs investigated in this work, it is expected that the precipitates will be dispersed homogeneously throughout the matrix, not clustered at the grain boundaries based on previous work by Khalil-Allafi *et al*. that showed that NiTi SMAs with Ni compositions of at least 50.6 atomic percent do not have a nucleation bias at the grain boundary.

Figures 16-18 show the results of the isobaric thermal cycling experiments for the polycrystalline samples 1-6, Table 2. These were tested incrementally either until 500 MPa or sample fracture. It is worth noting that sample 5 broke in the pin hole region, not in the gage section. For each of these samples, the transformation strains, R-phase

formation, irrecoverable strain, transformation temperatures, and thermal hysteresis varied.

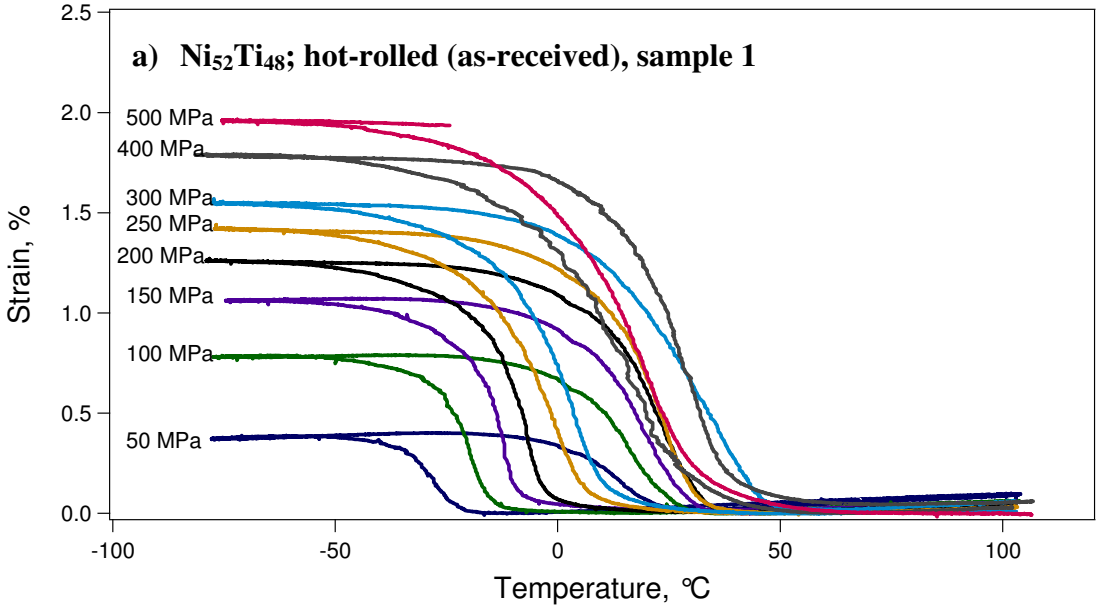

Figure 16. Isobaric thermal cycling experimental results for the polycrystalline $Ni_{52}Ti_{48}$ samples that were aged under no constraint. The results include a) sample 1: hot-rolled (as-received) b) sample 2: hot-rolled then aged at 450°C for 5 hrs, and c) sample 5: hot-rolled, solution heat treated at 900°C for 1 hr followed by aging at 450°C for 5 hrs.

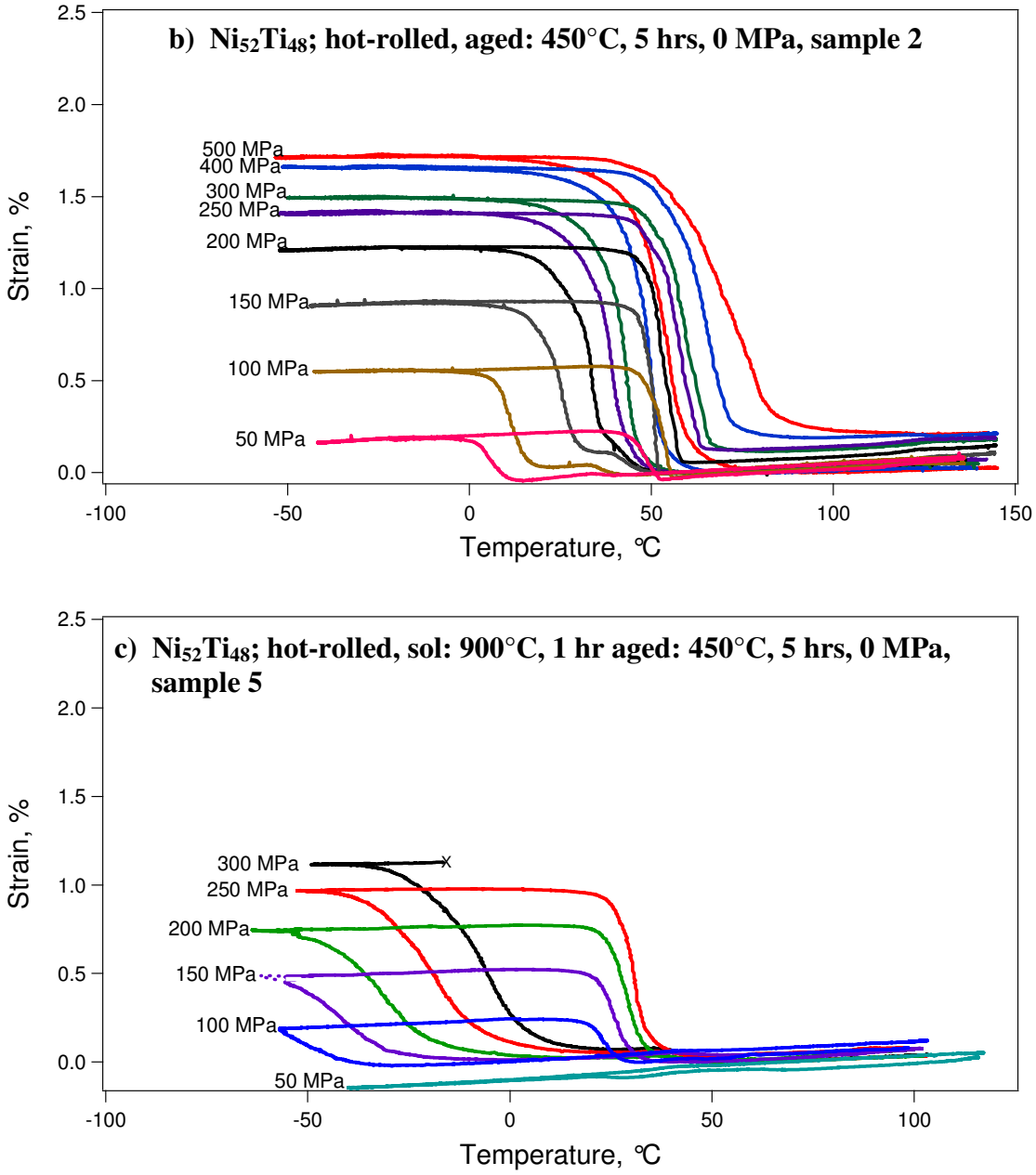

Figure 16. Continued

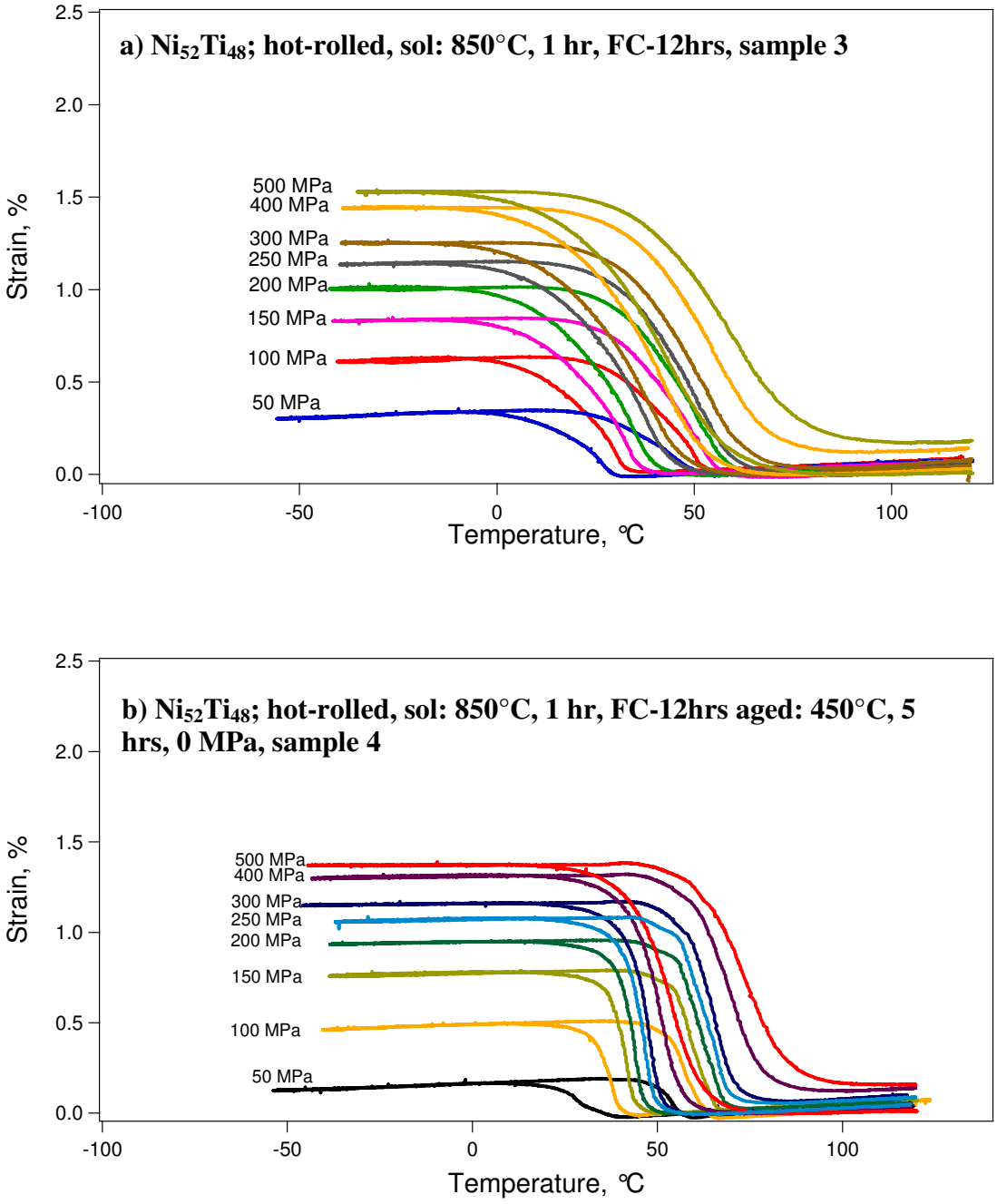

Figure 17. Isobaric thermal cycling experimental results for the polycrystalline $Ni_{52}Ti_{48}$ samples that were solution treated at 850°C for 1 hr then furnace cooled for 12 hrs. The results include a) sample 3: hot-rolled, solution heat treated and b) sample 4: hot-rolled, solution heat treated at 850°C for 1 hr then furnace cooled for 12 hrs, followed by aging at 450°C for 5 hrs.

Figure 18b shows the strain-temperature response of sample 6 while the sample was subjected to a 50 MPa tensile stress. An R-phase martensitic variant that resulted in a compressive transformation strain was biased even though an external tensile stress was applied. Upon completion of the R-phase transformation, a thermal contraction of R-phase took place. At M_s, the R-phase to B19' transformation begins. The sample does not appear to have transformed to the R-phase during the reverse transformation. The transformation strains, which will be discussed in detail later, were -0.06% and 0.15%, for the R-phase and B19' martensite phases, respectively. While the overall transformation strains were rather small it is evident that different types of variants, resulting in compressive or tensile transformation strains form independently of one another. Aging under 0 MPa leads to the formation of R-phase variants yielding to overall tensile strains, under relatively low external tensile stresses, however, aging under tensile stresses cause the formation of R-phase variants that result in compressive transformation strains under relatively low external tensile stresses.

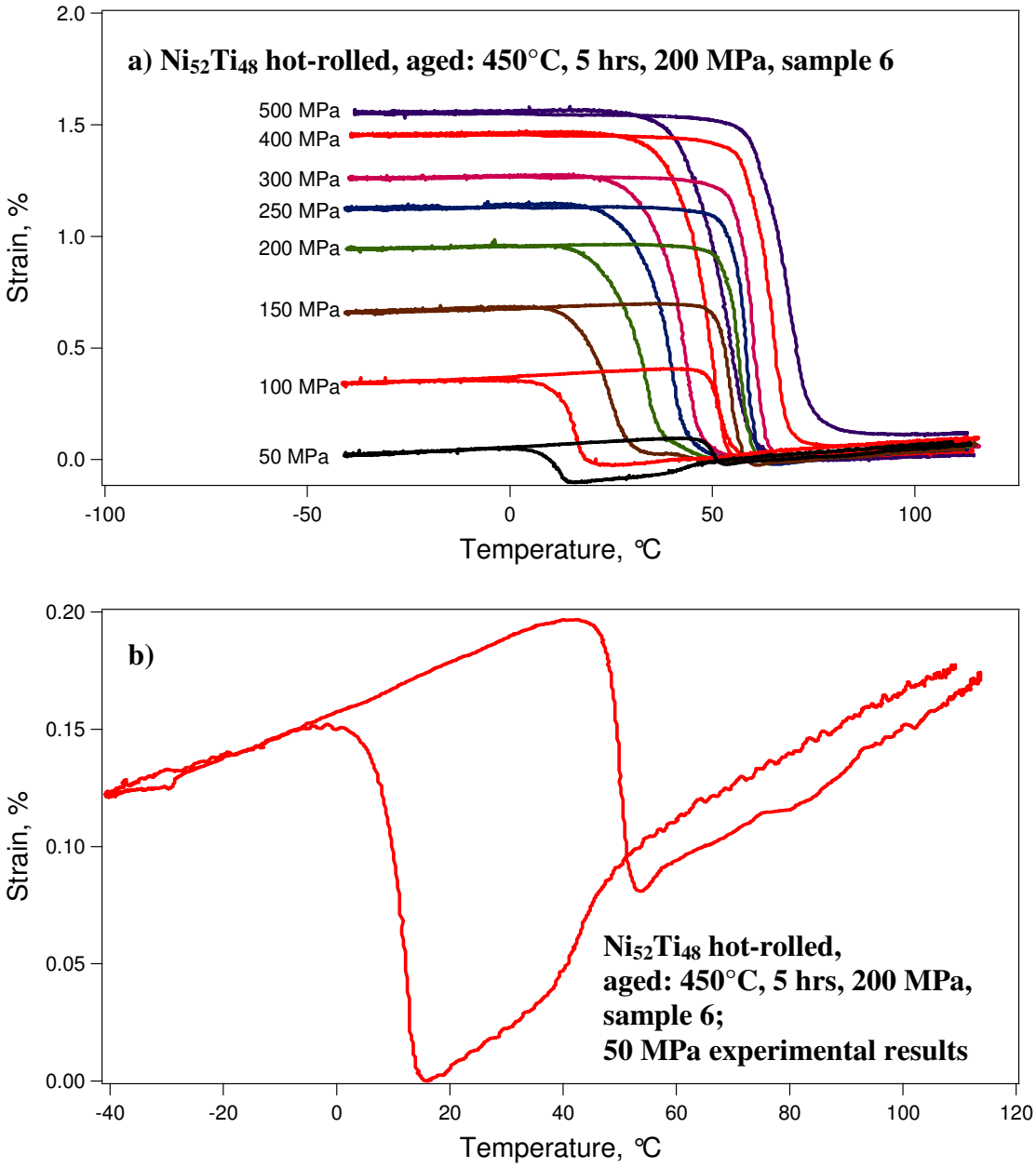

Figure 18. Isobaric thermal cycling experimental results for the polycrystalline $Ni_{52}Ti_{48}$ sample that was hot-rolled then aged at 450°C for 5hrs under a 200 MPa tensile stress. a) all experimental results. b) 50 MPa experimental result.

For the TWSME comparison, samples 6 – 8 were also investigated in addition to the samples introduced above that were subjected to the incrementally increasing tensile stresses. Figure 19 shows the strain-temperature response from the isobaric load bias experiments for each polycrystalline sample under 0 MPa. The results confirm that samples 1 and 3 show no clear signs of transformation. This was expected because these samples were not subjected to any training or constrained aging processes. Samples 2, 4, and 5 showed very minimal signs of transformation. Since these samples were not aged under a bias stress, it was expected that four precipitate variants would be present within the SMA microstructure. The internal stress of these precipitant variants would negate each other producing insufficient oriented internal stress in order to bias a specific martensite variant. This was not entirely the case. Sample 2 produced a -0.11% transformation strain. Sample 4 underwent a series of tensile and compressive transformation strains during the reverse transformation. Sample 5 produced a -0.04% transformation strain. However in this group of samples, the temperature hysteresis was either very large, approximately 20°C, or there was no real corresponding back transformation to correspond to the forward transformation. The back transformation occurred gradually over a temperature range.

Samples 6-9, under 0 MPA, first thermally contracted, and then underwent an R-phase transformation that resulted in a compressive transformation strain. Upon completion of the R-phase transformation, samples 6 and 8, continued to thermally contract, whereas samples 7 and 9 either began to detwin or continued the transformation of previously

untransformed portions of the matrix, likely in addition to thermal contraction. The magnitude of the transformation strains increased with decreasing temperature. The stress required to create a macroscopic strain transformation stems from internal stresses caused by precipitates, dislocations, and other internal defects. From this, we can assume that sample 8 experienced the greatest amount of internal stress, followed by samples 7, 9 then 6.

Samples 6-9 showed partial TWSME by consistently transforming to the R-phase, however these samples did not transform to the B19' martensite phase as expected or the B19' transformation did not result in any external strain. Figure 20 shows samples 6-9 superimposed for a better comparison. The oriented internal stress fields were able to bias a single R-phase variant to varying degrees. Samples 7 and 9 behaved very similarly during the forward and reverse transformation. Each underwent comparable strain transformations but had varying transformation start and finish temperatures, with sample 9 having the higher start and finish temperatures. This can be expected because the samples were aged at different aging temperatures. As mentioned in the previous chapter, R_s is only affected by aging temperature, not sample composition or aging time. Sample 8 showed a lower transformation temperature when compared to samples 7 and 9. The precise reason for this is unclear as samples 6, 7, and 8 were aged at the same temperature thus, we would expect for R_s to be the same in each of these samples. A possible reason for the delayed transformations in both the forward and reverse transformations could be how the 100 MPa applied stress during aging affected the

precipitate formation. Therefore, another method of further controlling the transformation temperatures could be through the application of varying external stresses during aging. However, further research is needed before this can truly be confirmed.

The thermal hysteresis of samples 7 and 9 were both less than 1.5°C. The thermal hysteresis of sample 6 and 8 were 3.3°C and 6.5°C, respectively. Since the magnitude of thermal hysteresis is a qualitative measure of frictional resistance to interfacial motion and stored elastic energy dissipation, samples 7 and 9 have a smaller resistance to interfacial motion. It appears that the hysteresis levels are closely related to the order in the microstructural features. One would expect for the higher aging stresses to produce a more aligned precipitates. If a stress is too high it is likely that no precipitates will form as the local stress throughout the entire matrix would have increased significantly.

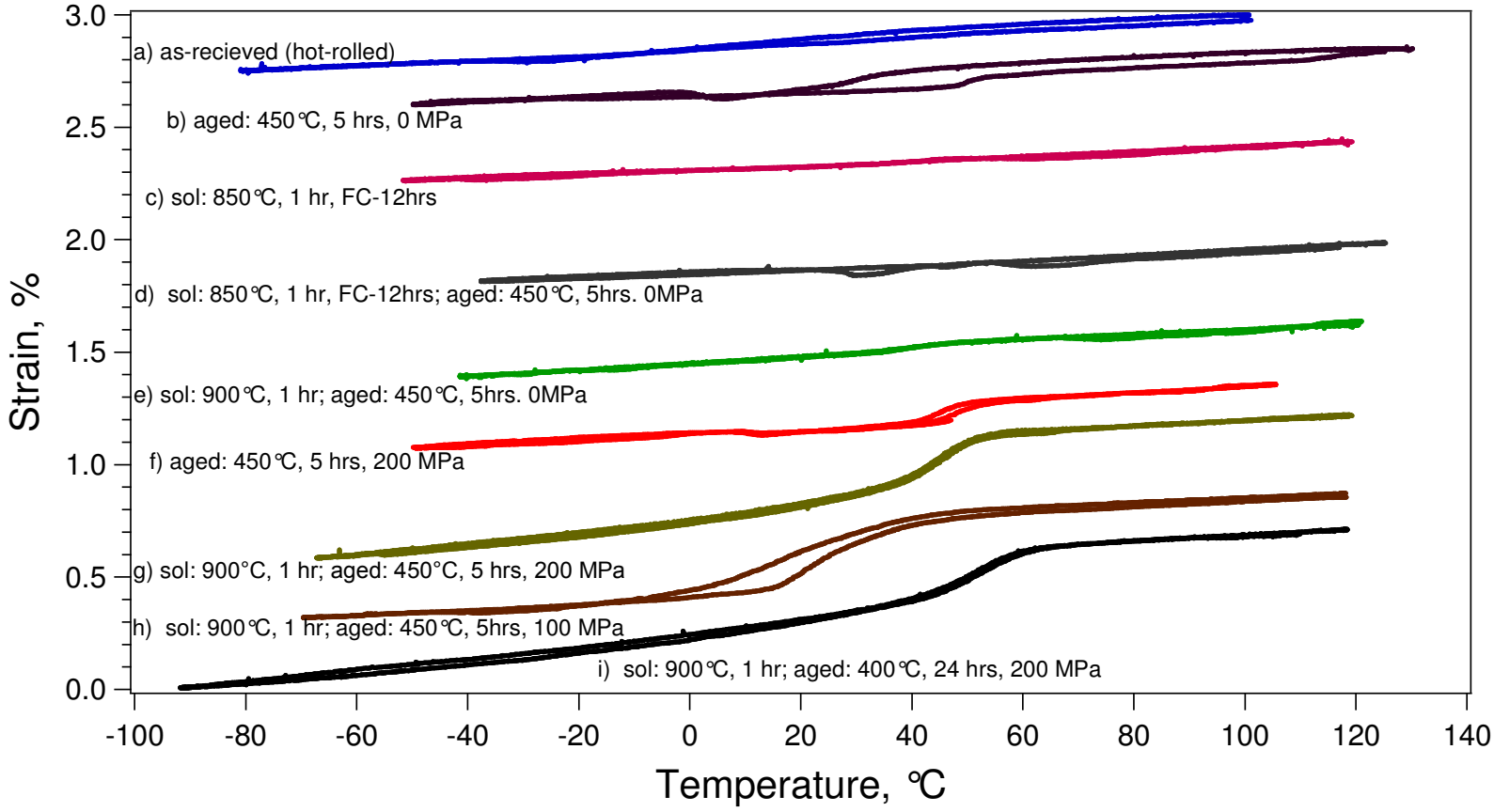

Figure 19. Strain-temperature curve results from the isobaric load bias experiments for $Ni_{52}Ti_{48}$ polycrystalline samples under 0 MPa. a) sample1: hot-rolled (as-received) b) sample 2:hot-rolled then aged at 450°C for 5 hrs, c) sample 3: hot-rolled, solution heat treated at 850°C for 1 hr , FC-12 hrs, d) sample 4: hot-rolled, solution heat treated at 850°C for 1 hr followed by aging at 450°C for 5 hrs, e) sample 5: hot-rolled, solution heat treated at 900°C for 1 hr followed by aging at 450°C for 5 hrs , f) sample 6: hot-rolled followed by aging at 450°C for 5 hrs under 200 MPa, g) sample 7: hot-rolled, solution heat treated at 900°C for 1 hr followed by aging at 450°C for 5 hrs under 200 MPa, h) sample 8: hot-rolled, solution heat treated at 900°C for 1 hr followed by aging at 450°C for 5 hrs under 100 MPa, and i) sample 9: hot-rolled, solution heat treated at 900°C for 1 hr followed by aging at 400°C for 24 hrs.

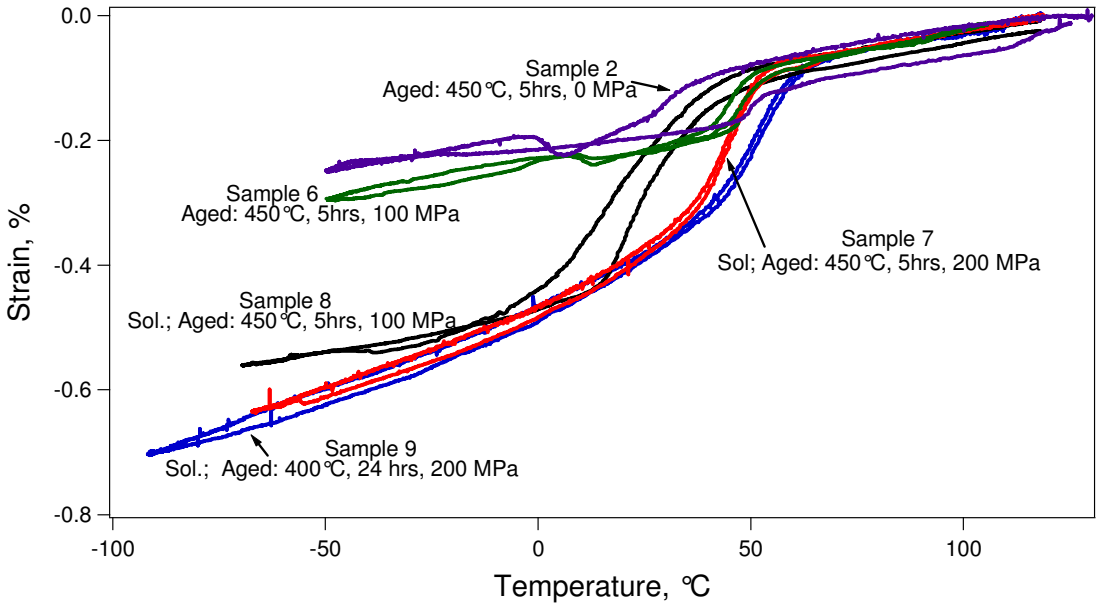

Figure 20. Strain-temperature curve results from the isobaric load bias experiments for $Ni_{52}Ti_{48}$ polycrystalline samples under 0 MPa with samples 6-9 superimposed for easier comparison.

Figure 21-Figure 23 show the phase diagrams for samples 1-6. The R-phase was expected to be seen in each aged sample; however, this was not the case. The R-phase was found in only samples 2, 5, and 6, the samples that were solution heat treated. The R-phase transformation strain increased with increasing applied stress, as shown in Figure 24. The R-phase appears to present in Sample 4 at 50 MPa. Since all the conditions except for the solution heat treatment were the same, it can be presumed that this is what brought about the R-phase differences, among others, between sample 4 and 5. From unpublished results from NASA Glenn Research Center it was expected for the transformation temperatures of sample 4 to be approximately 37°C, 27°C, 12°C, 38°C, and 45°C for R_s, M_s, M_f, A_s, and A_f respectively. From these results it was apparent that

R-phase was present in both the forward and reverse transformation, however, the R-phase transformations occurred close to the B19' transformation temperature, with the R_f and M_s transformation temperatures being indistinguishable. Therefore, it is likely that at low stress levels, less than 100 MPa, the R-phase is present in the material.

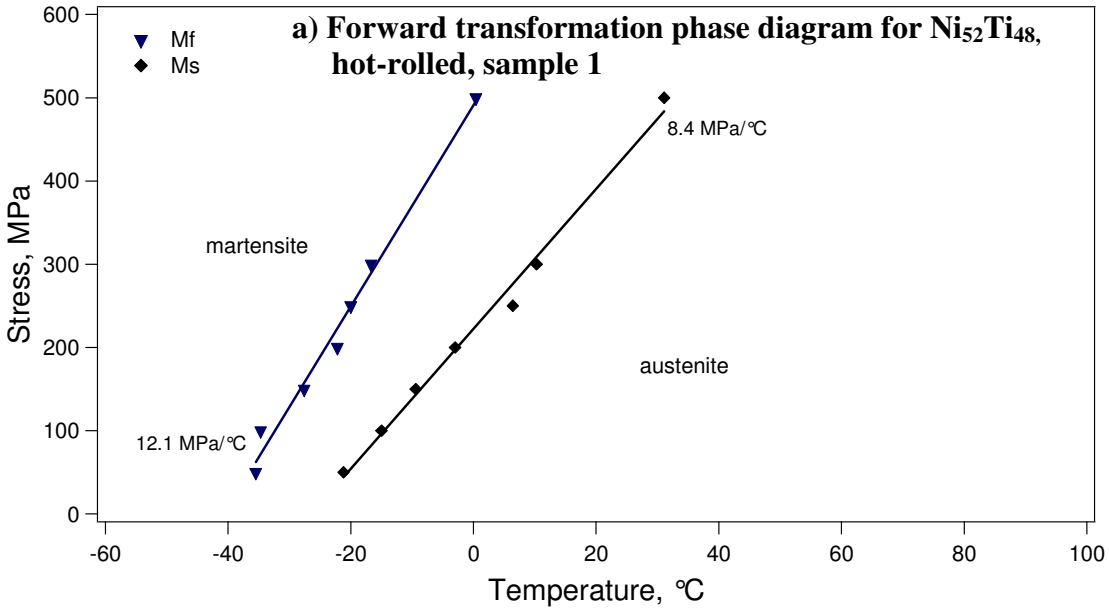

Figure 21. Stress vs. temperature phase diagram of $Ni_{52}Ti_{48}$ polycrystalline samples 1, 2, and 5. a) sample 1 forward transformation, b) sample 1 reverse transformation, c) sample 2 forward transformation, d) sample 2 reverse transformation, e) sample 5 forward transformation, and f) sample 5 reverse transformation.

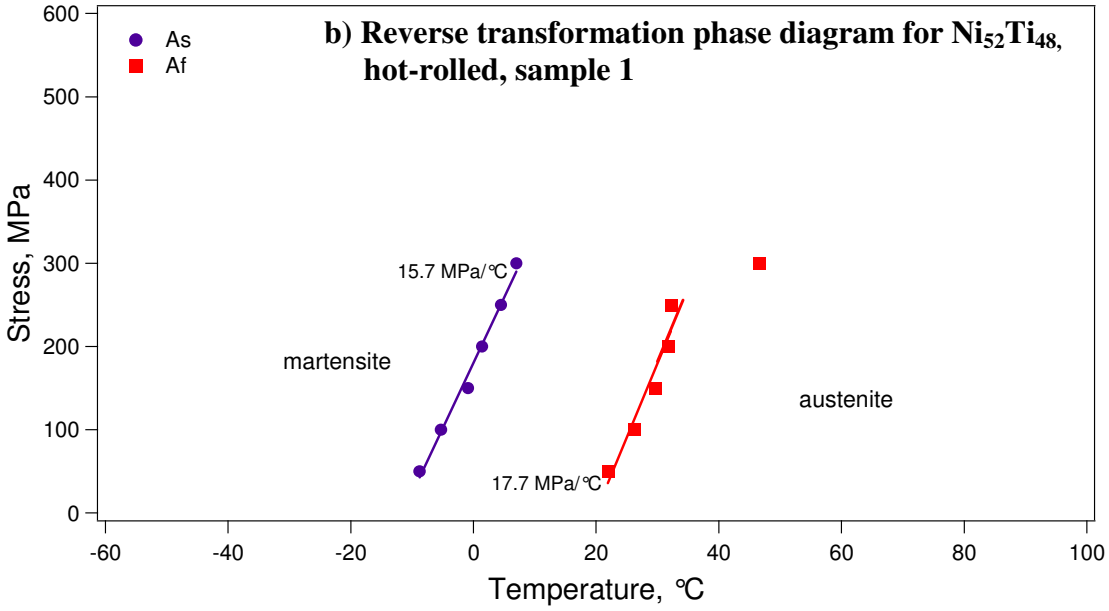

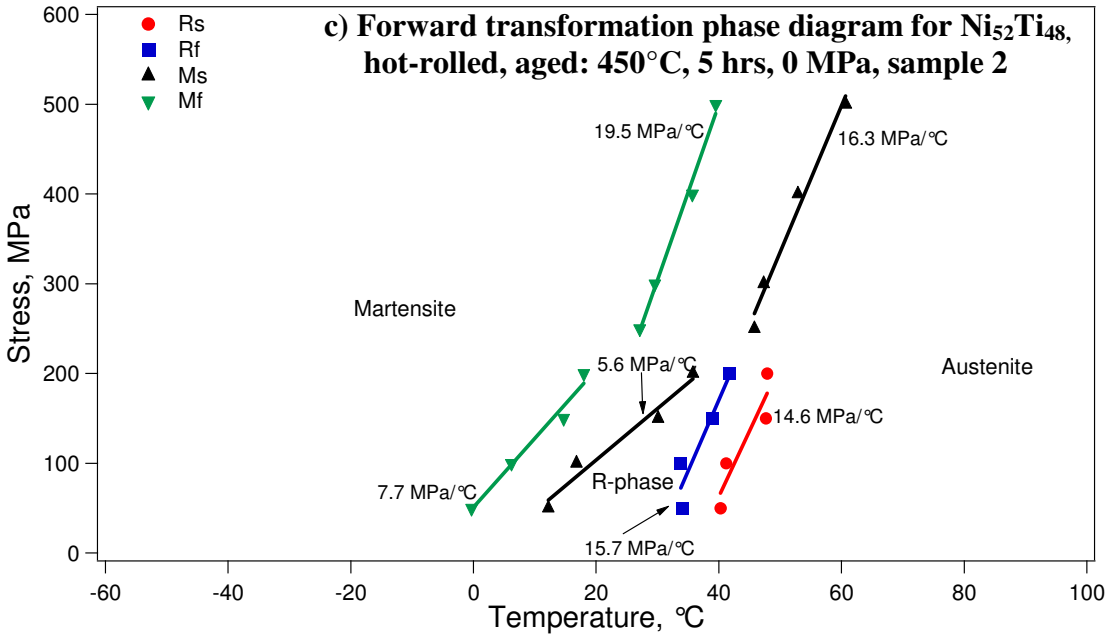

Figure 21. Continued

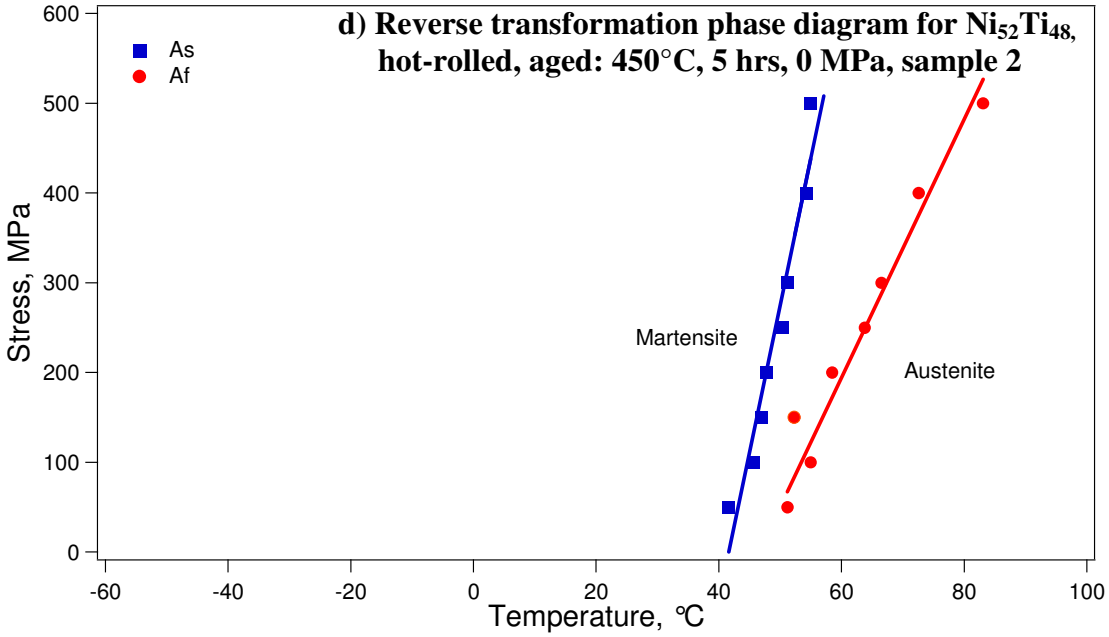

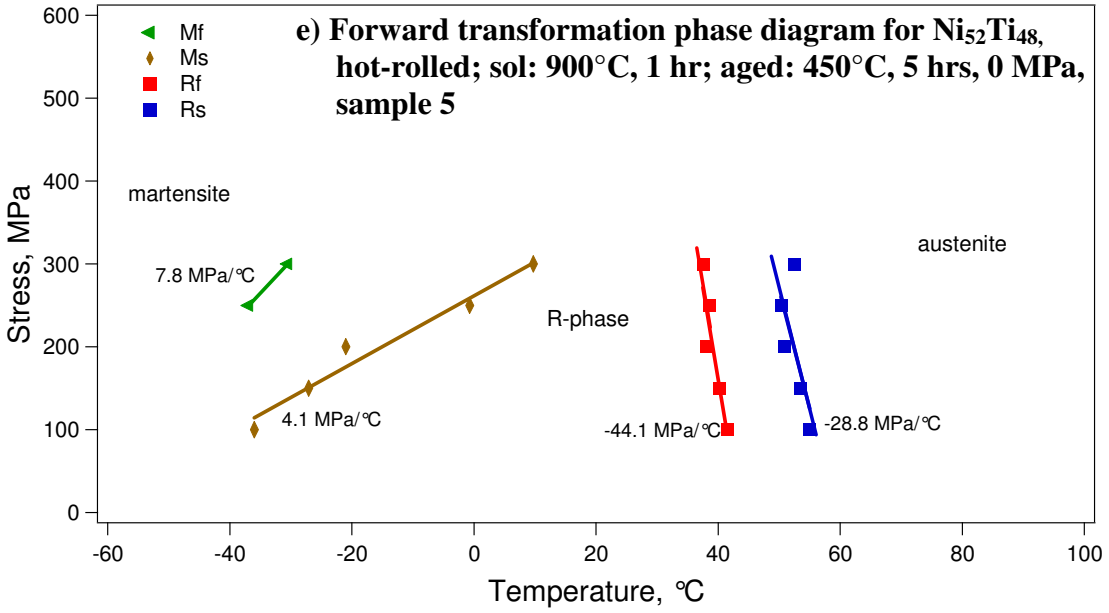

Figure 21. Continued

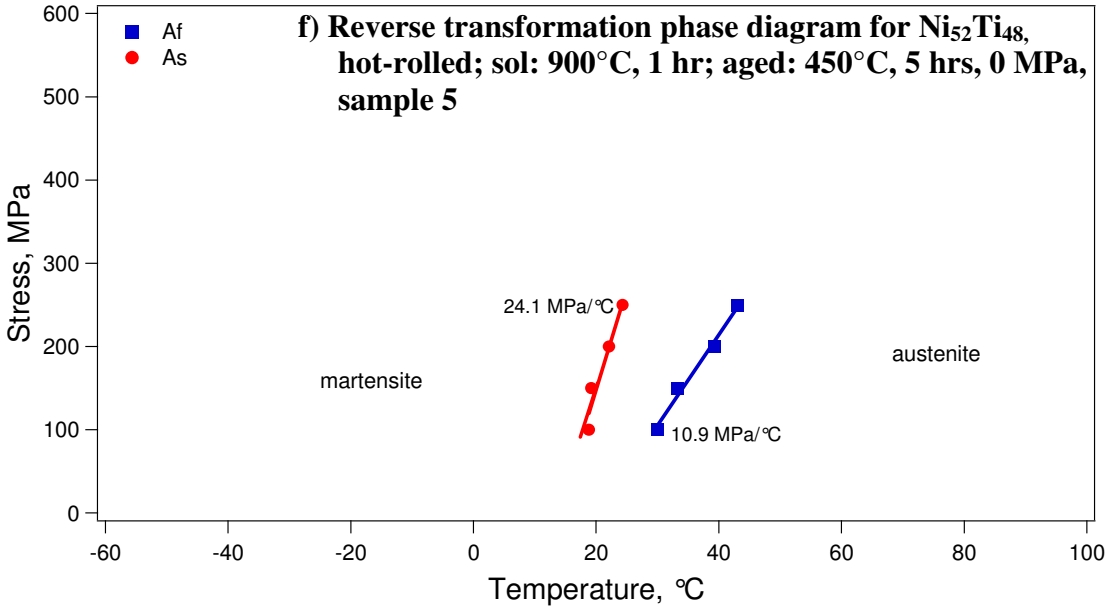

Figure 21. Continued

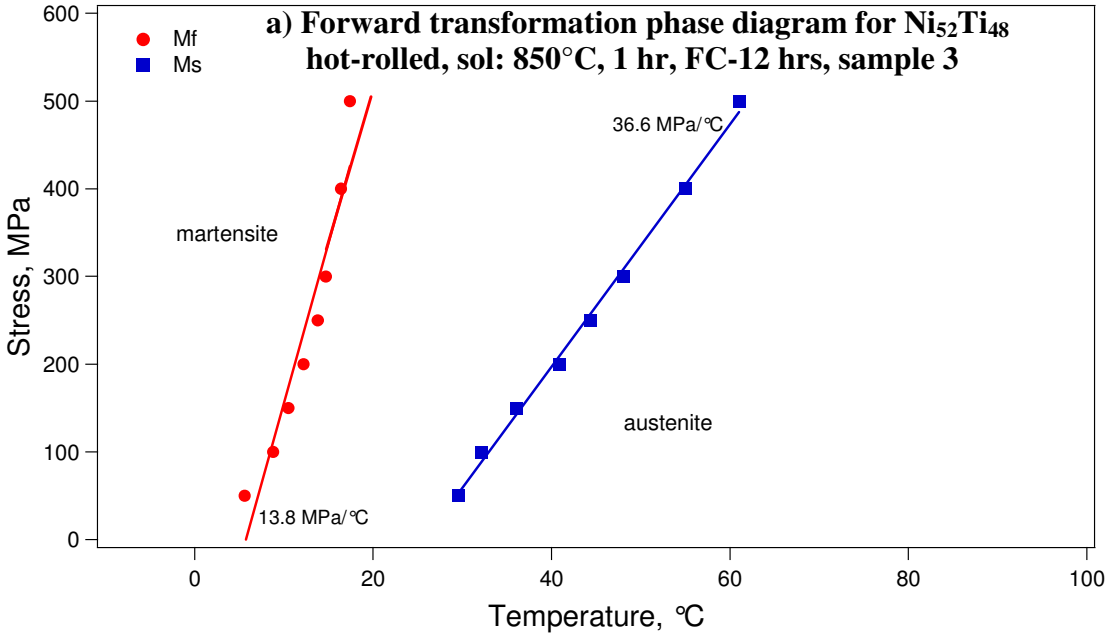

Figure 22. Stress vs. temperature phase diagram of $Ni_{52}Ti_{48}$ polycrystalline samples 3 and 4. a) sample 3 forward transformation, b) sample 3 reverse transformation, c) sample 4 forward transformation, and d) sample 4 reverse transformation.

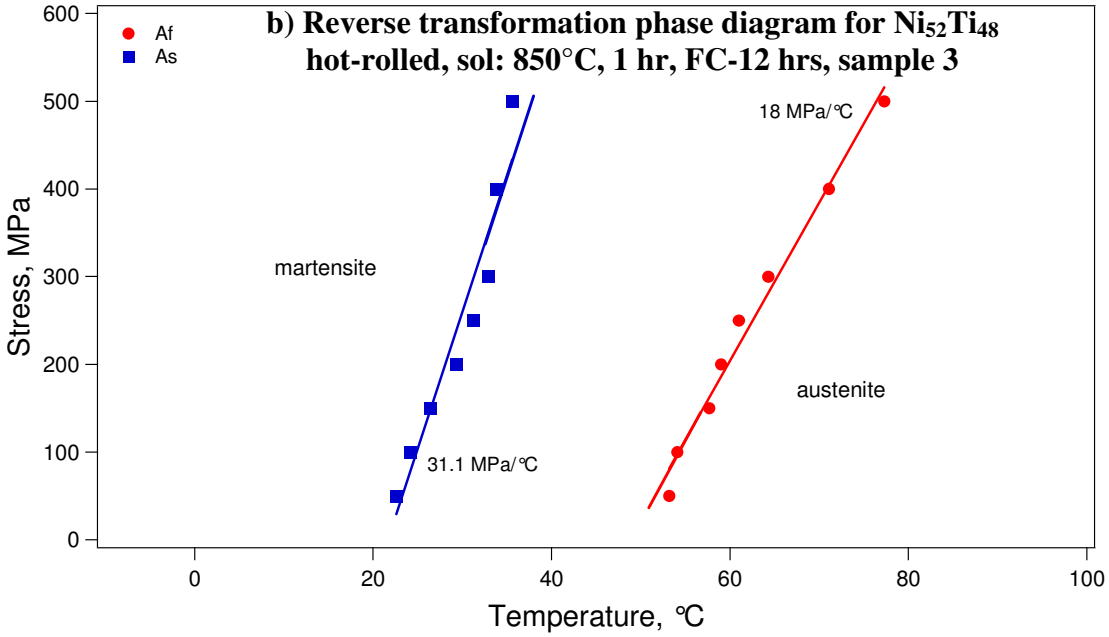

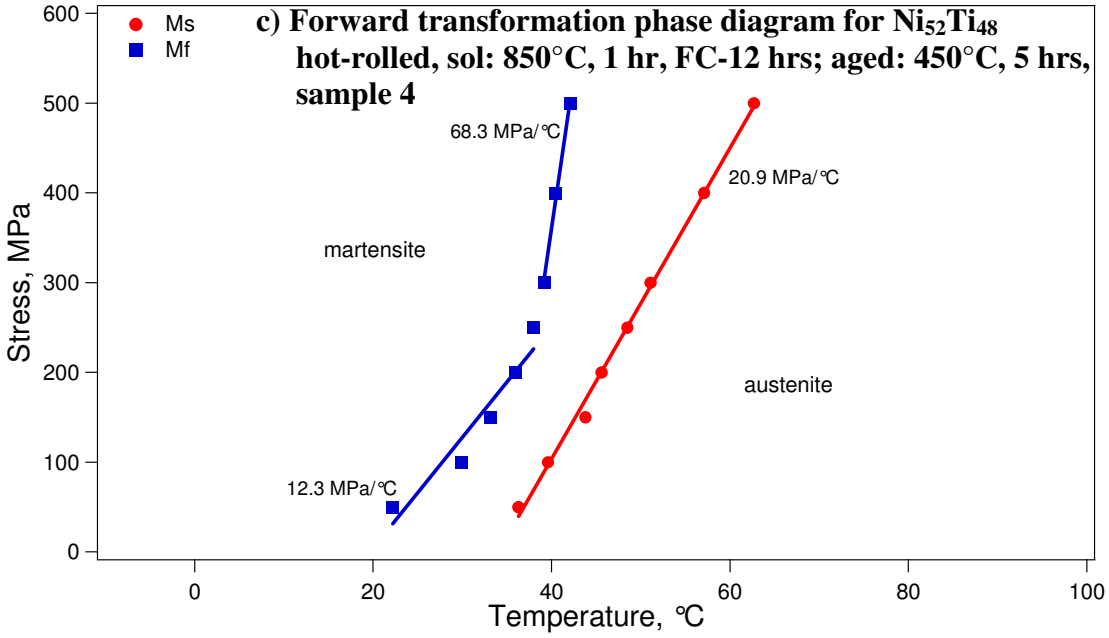

Figure 22. Continued

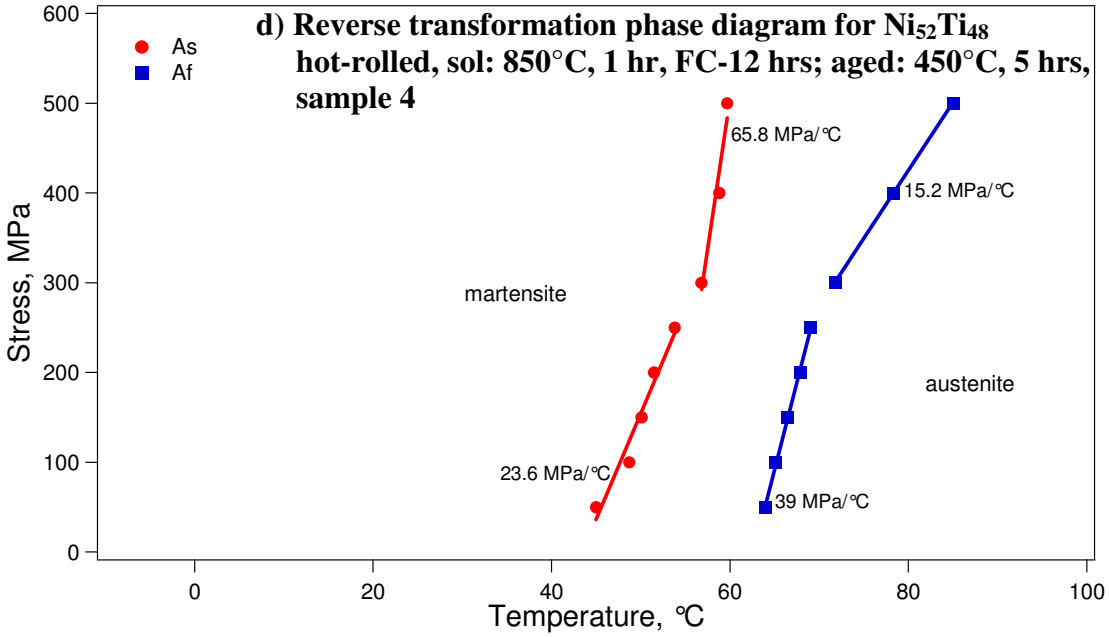

Figure 22. Continued

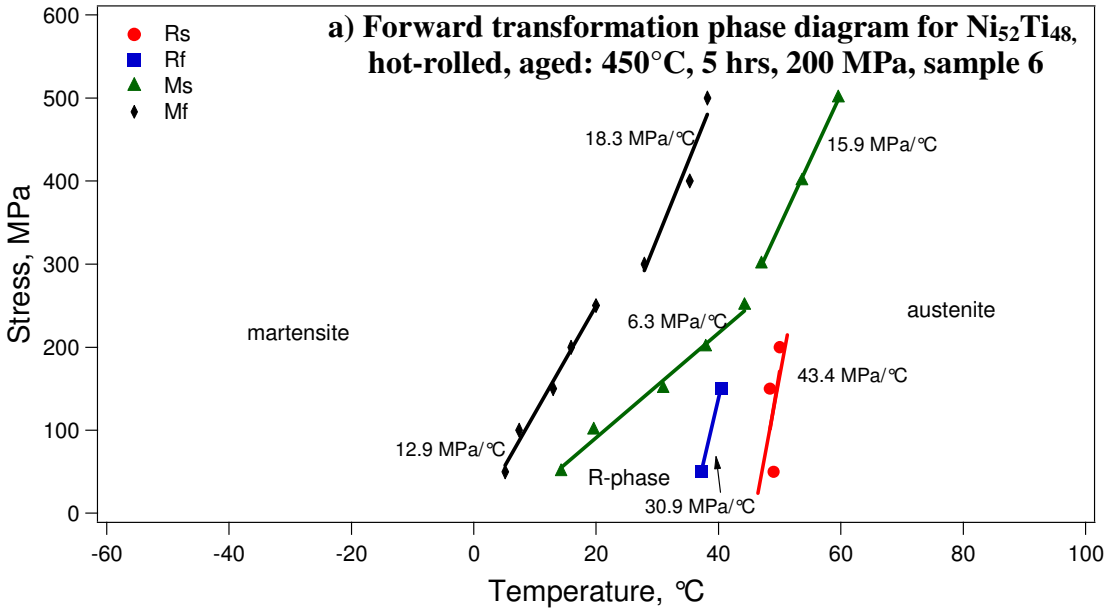

Figure 23. Stress vs. temperature phase diagram of $Ni_{52}Ti_{48}$ polycrystalline sample 6. a) sample 6 forward transformation, b) sample 6 reverse transformation.

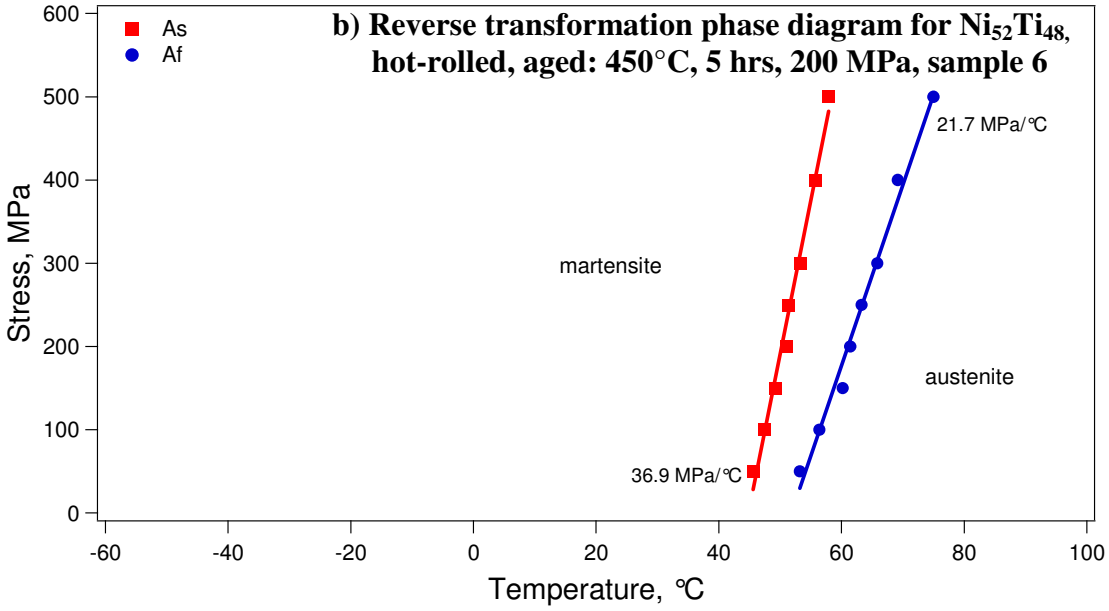

Figure 23. Continued

The various solution and aging heat treatments had varying effects on the transformation temperatures of each of the samples. Samples 1 and 5 had the lowest martensite transformation temperatures. The transformation temperatures of sample 4 increased by approximately 20°C with aging, over sample 3. For this reason, the hot-rolled then solution heat treated sample at 900°C sample was not tested, because it was expected that the transformation temperatures of the sample would be lower than sample 5. Sample 4, in Figure 22e shows two different M_f transformation rates. This type of behavior was typically seen when R-phase was present, however, from the isobaric thermal cycling results, R-phase did not appear to be present. The transformation rate changed at approximately 300 MPa.

The R-phase transformation temperatures decreased with increasing applied stress for sample 5 as shown in Figure 21e. This was the only sample that behaved in this manner. The martensite transformation temperatures increased with increasing applied temperature.

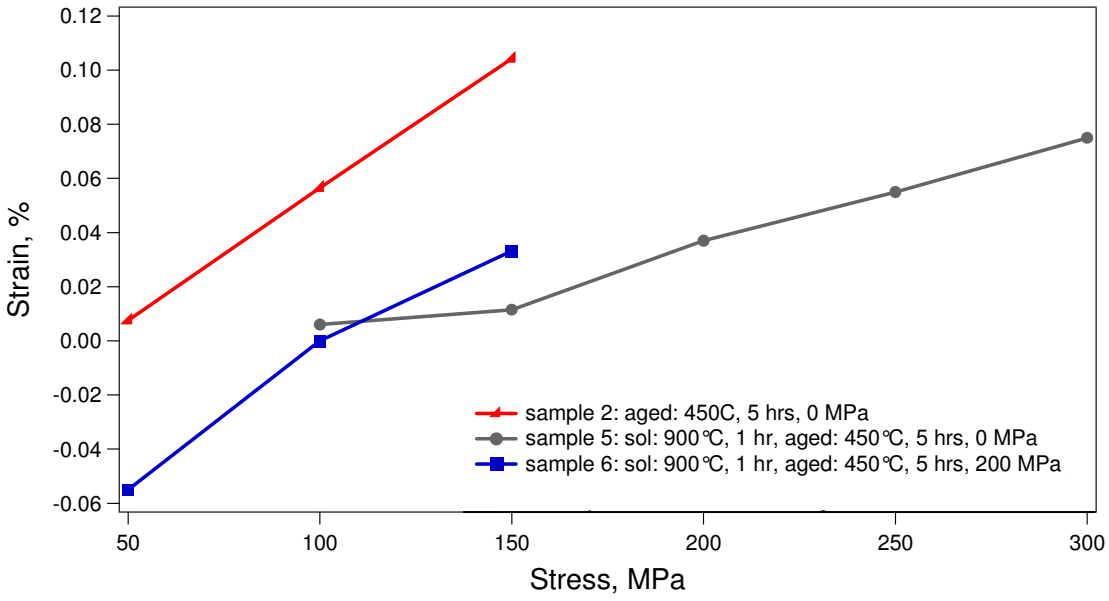

Figure 24. R-phase transformation strains for samples 2, 5, and 6 of the $Ni_{52}Ti_{48}$ polycrystalline samples.

Figure 25 shows the thermal hysteresis response for samples 1-6. Sample 5 showed the highest thermal hysteresis when compared to samples 1-6, approximately 20-30°C higher depending on the applied stress level. Possible reasons for the large temperature hysteresis increase include sample 5 being peak aged thus yielding higher coherency strains in the expected 4 precipitate variants produced during aging. The strain-temperature loops are quite asymmetric in sample 5 as compared to that of the other

samples indicating that the nucleation of austenite is quite difficult. Although the exact reason for this is not known at this point it is likely to be related to the necessity of geometrically necessary martensite twins that needs to form between coherent precipitates before transformation back to austenite which requires additional overheating. Considering that this is the only sample that was water quenched directly after being subjected to the solution heat treatment, this is likely causing the delayed martensitic transformation. According to Hamilton *et al.*, a large temperature hysteresis is associated with increased frictional resistance to interfacial motion. [8] The solution heat treatments will be correlated to the sample microstructures later in the chapter.

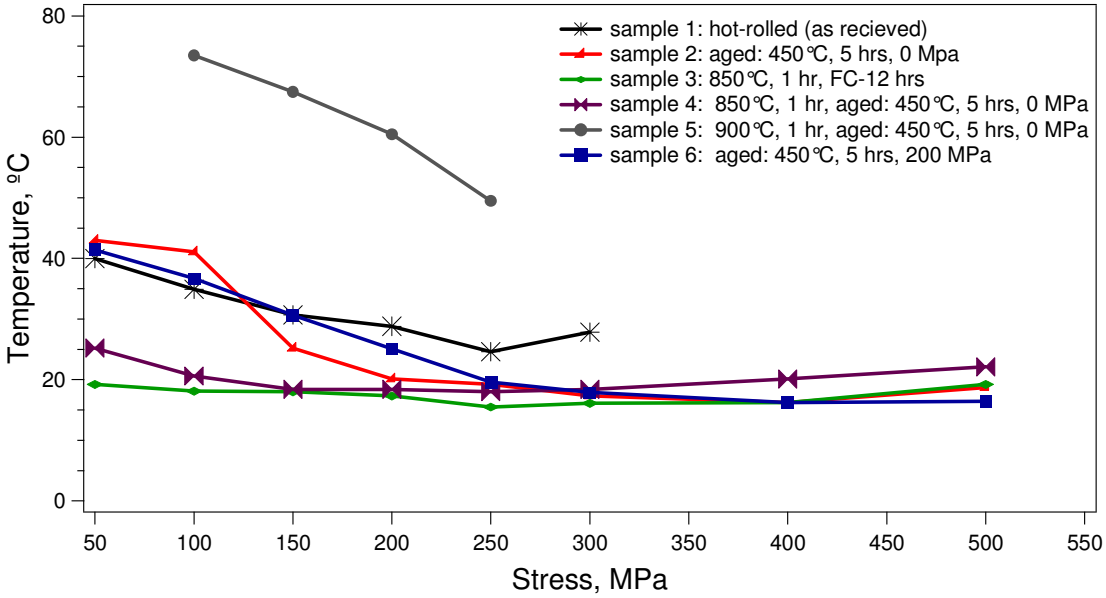

Figure 25. Temperature hysteresis values for samples 1-6 of the $Ni_{52}Ti_{48}$ polycrystalline samples.

Recall that two different solution heat-treatments were used throughout the study of the polycrystalline samples. These solution heat treatments affected the samples differently.

Microstructural Investigation

First, considering the microstructural effects of the furnace cooling samples over quenching immediately upon completion of the solution heat treatment allows various precipitates with different sizes to form with the sample microstructure as the sample cools. Samples that are water quenched immediately stop the treatment process and no precipitates are expected. Therefore, the samples that were furnace cooled formed new precipitates whereas the sample samples that were water quenched were able to dissolve much of the prior Ni_4Ti_3 precipitates. The main difference in selecting solution heat treatment temperatures is the that there is a direct relationship between the solution heat treatment time, temperature, grain size, and precipitate state. The longer that sample is allowed to solution heat treated, the larger the grains will be.

Sample 1, the as received hot-rolled sample, underwent the largest transformation strain, as can be seen in Figure 26, and was able to resist irrecoverable strain until higher stresses, Figure 27, when compared to samples 2 – 6 except for samples 3 and 6.

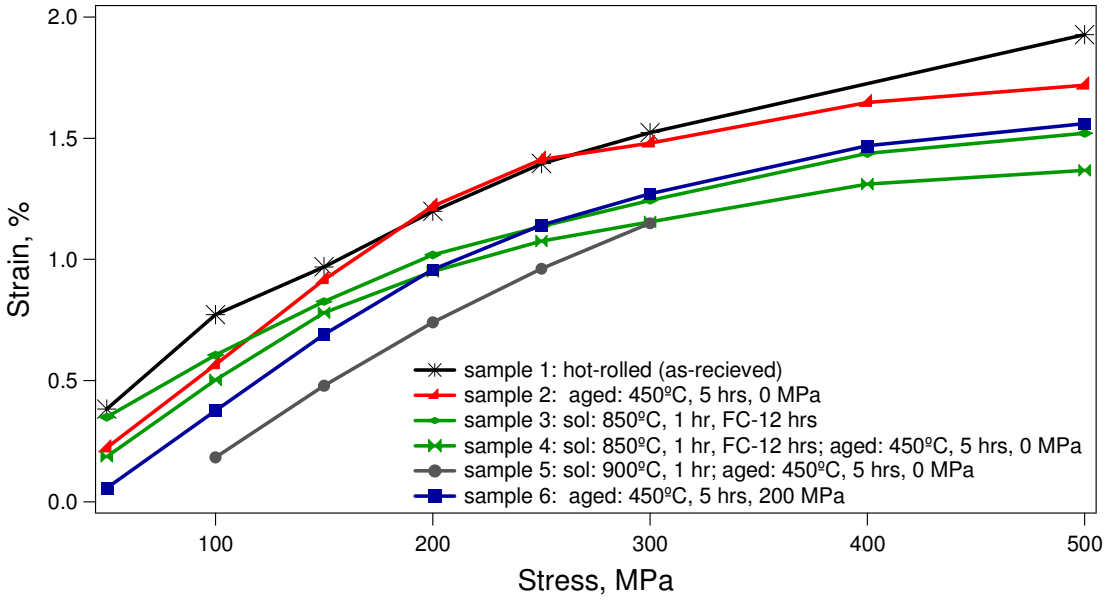

Figure 26. Total transformation strains for samples 1-6 of the $Ni_{52}Ti_{48}$ polycrystalline samples.

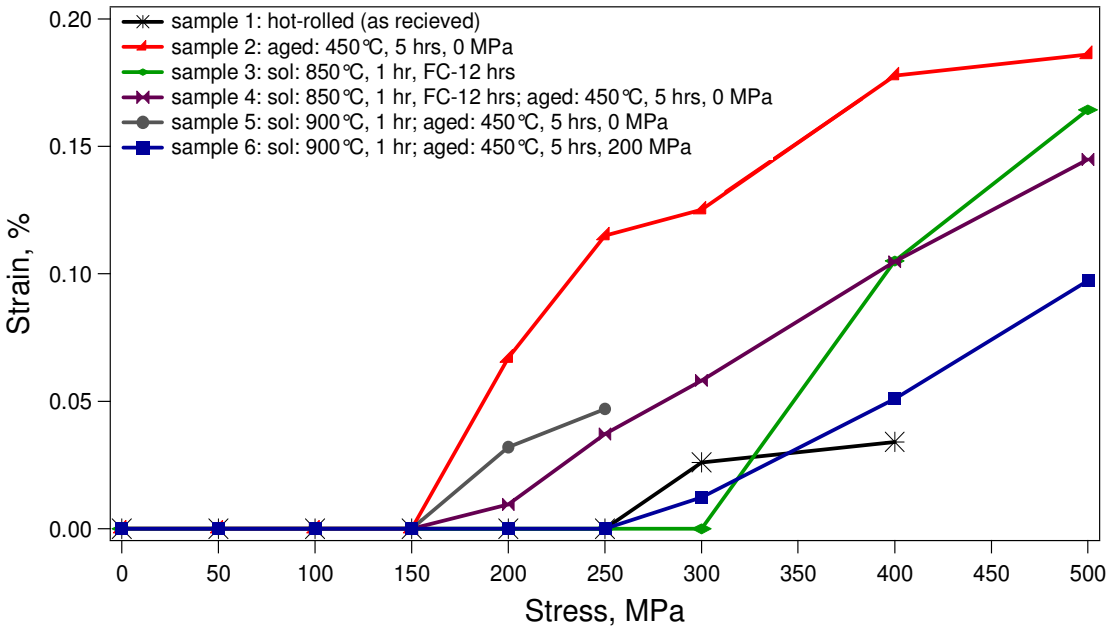

Figure 27. Irrecoverable strains experienced by samples 1-6 of the $Ni_{52}Ti_{48}$ polycrystalline samples.

After looking at Figure 28a and b it is clear that the grain size increased after the sample was subjected to the 900°C, 1 hr solution heat treatment. The grain sizes were approximately 100 µm and 130 µm for sample 1 and the 900°C solution heat treated sample, respectively. From the Hall-Petch relation that relates the size of the grain boundary to the yield strength of a material, solution heat treating the polycrystalline samples decreases the yield stress of said samples. Therefore, in a number of the solution and aging heat treatment cases studied in this study, there was a decrease in the stress level at which irrecoverable strain was observed, which can be correlated to the grain size.

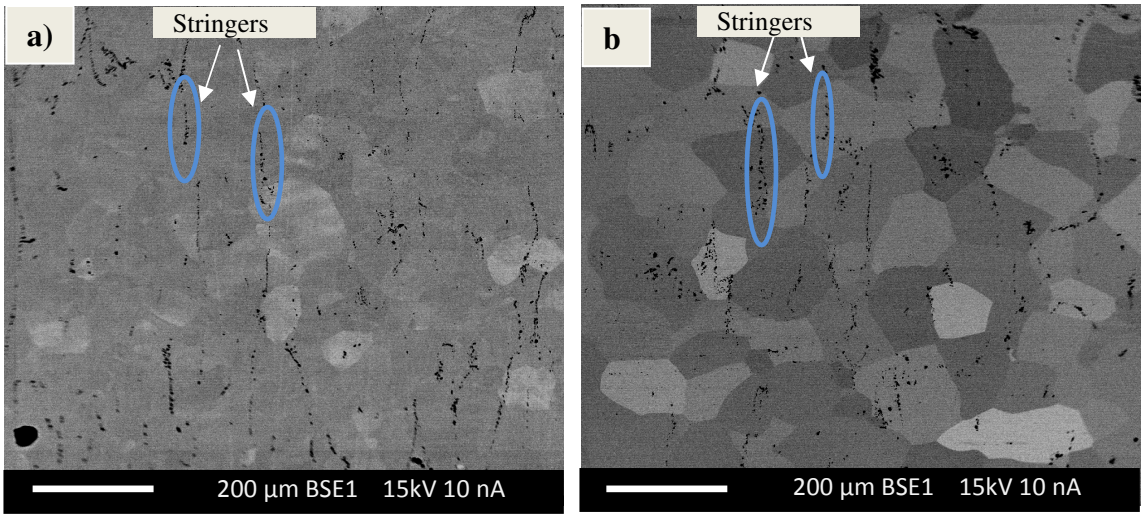

Figure 28. SEM images taken of the a) hot-rolled (as-received) sample and b) 900°C solution heat treated water quenched sample.

Also present in Figure 28 a and b are stringers that are oriented along the rolling direction. The stringers, or inclusions, were formed during the casting process and consist of oxides such as $Ni_4Ni_2O_x$ and TiO_2. While these stringers are secondary

phases, they do not provide the necessary internal stresses required to produce TWSME because they are incoherent and quite large. These secondary phases also do not take part in the solid-to-solid phase transformation. The Ni_4Ti_3 precipitate formation was locally unaffected by the presence of stringers.

Figure 29 a and b shows the microstructure of samples 1 and 2, respectively. The dominant plate like phase in Figure 29 a and b are the Ni_4Ti_3 precipitates. It is clear that the precipitate is homogeneously distributed throughout the grains. Multiple precipitate variants are present, however the precipitates appear coarse. Ni_3Ti precipitates were present along the grain boundaries and within grain boundaries. As mentioned in the introduction, Ni_3Ti typically form when Ni-rich NiTi has been aging for a long period of time, therefore, although samples 3 and 4 were aged for 1 hour at 850°C, they continued to be aged during the 12 hour furnace cooling time period. The area immediately surrounding the Ni_3Ti precipitates appears to be void of Ni_4Ti_3 precipitates. This is most likely attributed to a compositional change surrounding Ni_3Ti precipitates. Upon further aging, Ni_4Ti_3 precipitates eventually formed, however, these precipitates were much smaller in size when compared to the Ni_4Ti_3 found within the matrix. From Figure 29, it is obvious that there is a high precipitate density in these samples. Since precipitates are incapable of participating in the solid-to-solid phase transformation, this leaves a much smaller portion of matrix that is capable of transforming. This, in part, can account for the small transformation strains experienced by the polycrystalline samples as shown above in Figure 26. It is worth noting that the Ni_3Ti precipitate was also present at low

levels in sample 1, the hot-rolled (as-received) sample. In sample 4, Ni_3Ti precipitates were present at a higher fraction than the hot-rolled sample, therefore the solution heat treatment time may be too long. A balance must be reached when selecting a solution heat treatment time in order that the previous Ni_4Ti_3 precipitates disappear while at the same time hindering the formation of Ni_3Ti precipitates.

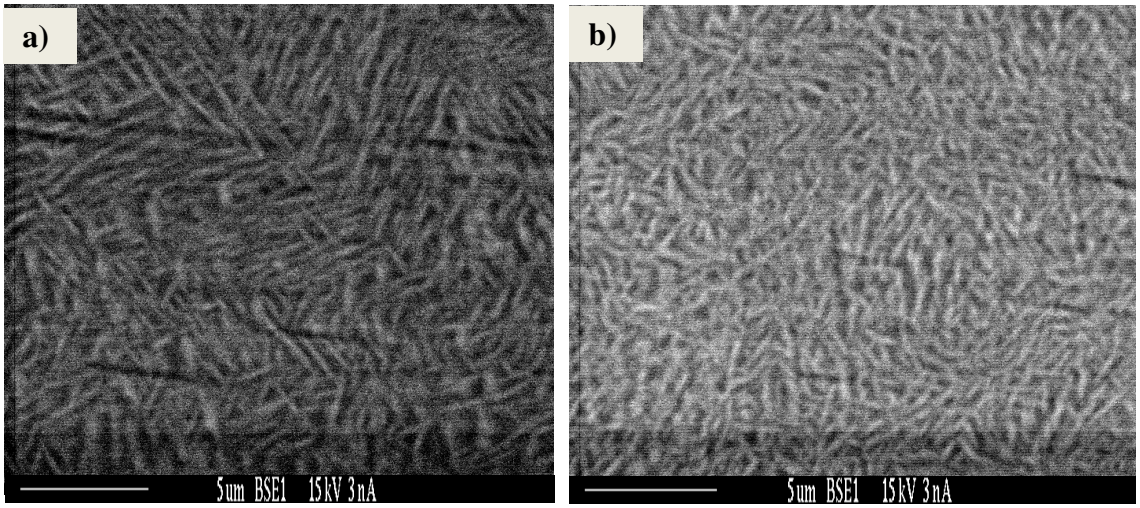

Figure 29. SEM image of $Ni_{52}Ti_{48}$ polycrystalline samples a) 1 and b) 2. The dominant phase in sample 2 are the Ni_4Ti_3 precipitates. The samples are at the same magnification.

The Ni composition of the $Ni_{52}Ti_{48}$ samples may, in fact, be too high in order to produce TWSME due to the large density of Ni_4Ti_3 precipitates produced during aging. This is because of the fact that once solution heat treated and water quenched, the M_s temperatures are too low and the selected heat treatments (450°C for 5 hours and 400°C for 24 hours) may not be sufficient to bring the transformation temperature high enough for practical temperature ranges to be able to measure TWSME.

Upon examination of the samples' microstructure, it is evident that when the hot-rolled, and furnace cooled samples were aged, this leads to the coarsening of the precipitates that were already present within the microstructure.

CHAPTER V

SUMMARY AND CONCLUSIONS

Single Crystalline $Ni_{50.6}Ti_{49.4}$

The shape memory behavior of single crystalline Ni-rich $Ni_{50.6}Ti_{49.4}$ bulk samples were investigated experimentally after subjecting the tensile samples to different aging heat treatments using isobaric thermal cycling experiments, superelasticity experiments, OM, and TEM. The samples were prepared using the Bridgman method, and then homogenized at 1000°C for 1hr then water quenched. The samples were then aged at 400°C for 1.5 hours under zero constraint (sample A), and tensile (sample B) and compressive (sample C) stresses of 150 MPa. The following conclusions were drawn from this portion of the study.

(1) The aging treatments produced precipitates and there were less than 30 nm in size. The precipitate variant orientation was indeterminable, using TEM, due to the high coherency stress field associated with the precipitates.

(2) The aging treatments used in this study bring about perfect dimensional stability during isobaric thermal cycling up to 400 MPa with the help of two stage transformations.

(3) Constrained aging does not affect the R-phase transformation temperatures and strain levels, however it can decrease the martensitic transformation strain levels. The martensitic transformation strain levels depend on the nature of the constraint.

(4) The onset of irrecoverable strain corresponded to the non-distinct regions of the R-phase temperature hysteresis. Non-distinct refers to regions of the R-phase temperature hysteresis where the hysteresis is not relatively constant or decreasing. This pattern was noticed regardless of the aging conditions.

(5) In samples A, B, and C1, TWSME strain is the highest in the unconstrained aging case where TWSME mainly originates from the R-phase transformation. However, in these samples constrained aging at 400 in the present composition did not lead to the desired large TWSME strain levels. Sample C2 successfully produced a 1.5% transformation strain.

(6) [112] and [114] twins in austenite transformed from [113] and [201] twins in martensite as a form of plastic deformation.

Polycrystalline $Ni_{52}Ti_{48}$

The shape memory behavior of polycrystalline Ni-rich $Ni_{52}Ti_{48}$ bulk samples were investigated experimentally after subjecting the tensile samples to different solution and aging heat treatments using isobaric thermal cycling experiments, OM, and SEM. The samples were received in hot-rolled condition. The samples were either solution heat-treated at 900°C for 1 hour then water quenched or 850°C for 1 hour then furnace cooled for 12 hours. The samples were then aged at 450°C for 5 hours under zero constraint, or tensile stresses of 100 and 200 MPa prior. One sample was aged at 400°C for 24 hours. The reader can refer to Table 2 for further processing details. The following conclusions were drawn from this portion of the study.

(1) Aging under stress can possibly be used to customize the martensitic transformation temperatures.

(2) Ni composition of alloy may be too high in order to bias a single B19' martensite variant and produce TWSME since transformation temperatures are too low.

(3) Constrained aging can easily bias R-phase variants and produce partial TWSME, however, further solution and aging heat treatment studies are needed in order to successfully bias B19' martensite variants.

(4) Water quenching immediately following a solution heat treatment prevents the formation of unwanted precipitates, whereas furnace cooling allows for the nucleation and growth of Ni_3Ti and Ni_4Ti_3 precipitates. Upon aging of furnace cooled samples, precipitates simply continue to grow.

(5) The high precipitate density prevented larger transformation strains.

CHAPTER VI

FUTURE WORK

Intermediate compositions between the ones investigated in this study, $Ni_{50.6}Ti_{49.4}$ and $Ni_{52}Ti_{48}$, should be subjected to select constrained aging heat treatments in order to successfully bias B19' martensite variants and find a compromise between the amount of Ni_4Ti_3 precipitates forming and the amount of reduction in transformation temperature due to Ni content. The effect of higher aging temperatures on $Ni_{52}Ti_{48}$ polycrystalline samples should be investigated in order to find the optimal transformation temperatures due to the matrix Ni content and the optimum precipitate size and coherency that would not suppress transformation temperatures significantly due to the coherency stress field and at the same time that would have enough coherency stress field to bias certain martensite variants for TWSME.

REFERENCES

[1] L. Chang, T. Read, Trans AIME 191 (1951) 47.

[2] K. Otsuka, X. Ren, Prog. Mater. Sci. 50 (2005) 511.

[3] H. Sehitoglu, R. Hamilton, D. Canadinc, X.Y. Zhang, K. Gall, I. Karaman, Y. Chumlyakov, H. J. Maier, Metall. Trans. A 34A (2003) 5.

[4] X. Zhang, J. Fernandez, J. Guilemany, Mater. Sci. Eng. A 438 (2006) 431.

[5] Miyazaki S, Otsuka K. ISIJ Int. 29 (1989) 353.

[6] M. Nishida, T. Honma, Scripta Metall. 18 (1984) 1293.

[7] K. Enami, A. Nagasawa, S. Nenno, Scripta Metall. 9 (1975) 941.

[8] R. Hamilton, H. Sehitoglu, Y. Chumlyakov, H. Maier, Acta Mater. 52 (2004) 3383.

[9] Yu.I. Chumlyakov, E.Yu. Panchenko, V.B. Aksenov, I.V. Kireeva, M.P. Kuksa, I. Karaman, H. Sehitoglu, J. Phys. IV France 115 (2004) 21.

[10] JF. Li, ZQ. Zheng, XW. Li, ZW. Peng, Mater. Des. 30 (2009) 314.

[11] J. Michutta, M. Carroll, A. Yawny, Ch. Somsen,K. Neuking, G. Eggeler Mater. Sci. and Eng. A 378 (2004) 152.

[12] P. Sittner, M. Landa, P. Lukas, V. Novak, Mech. Mater. 38 (2006) 475.

[13] M. Nishida, C. Wayman, Scripta Metall. 18 (1984) 1389.

[14] K. Otsuka, C.M. Wayman, Shape Memory Materials, first ed., Cambridge University Press, Cambridge, 1998.

[15] Y. Chumlyakov, E. Panchenko, I. Kireeva, S. Efimenko, V. Aksenov, H. Sehitoglu, Dokl. Phys. 47 (2002) 510.

[16] D. Y. Li, L. Q. Chen, Acta Mater. 45 (1997) 471

[17] Y.I Chumlyakov, S.V Starenchenko, J. Phys. IV C8 (1995) 803.

[18] D. Treppman, E. Hornbogen, J. Phys. IV C2 (1995) 211.

[19] K. Gall, H. Sehitoglu, Y. Chumlyakov, Y. Zuev, I. Karaman, Scripta Mater. 39 (1998) 699.

[20] M. Nishida, C.M. Wayman and T. Honma, Metall. Trans. 17A (1986), 1505.

[21] J. Khalil-Allafi, G. Eggeler, W. Schmahl, D. Sheptyakov, Mater. Sci. Eng. A 438-440 (2006) 593.

[22] S.Miyazaki, K.Otsuka, Y.Suzuki, Scripta Metall. 15 (1981) 287.

[23] A. Ishida, S. Miyazaki, Trans ASME. 121 (1999) 2.

[24] X. Zhang, H. Sehitoglu, Mater. Sci. Eng. A A374 (2004) 292.

[25] G. Tan, Y. Liu, P. Sittner, M. Saunders, Scripta Mater. 50 (2004) 193.

[26] J. Shaw, S. Kyriakides, J. Mech. Phys. Solids 43 (1995) 1243.

[27] T.W. Duerig, Mater. Sci. Eng. A 438-440 (2006) 69.

[28] W.J. Moberly, J.L. Proft, T.W. Duerig, R. Sinclair, Mat. Sci. For. 56 (1990) 605.

[29] S. Ii, K. Yamauchi, Y. Maruhashi, M. Nishida, Scripta Mater. 49 (2003) 723.

[30] J.X. Zhang, M. Sato and A. Ishida, Acta Mater. 49 (2002) 3001.

[31] J.X. Zhang, M. Sato and A. Ishida, Phil. Mag. A 82 (2002) 1433.

[32] Khalil-Allafi J, RenX, Eggeler G. Acta Mater. 50 (2002) 793.

VITA

Name: Fatmata Haja Barrie

Address: Texas A&M University, Department of Mechanical Engineering,
3123 TAMU
College Station, TX 77843-3123

Email Address: fbarrie@gmail.com

Education: B.S., Mechanical Engineering with an additional major in International Relations, Carnegie Mellon University, 2007
M.S., Mechanical Engineering, Texas A&M University, 2009